Quaternary Science Reviews 246 (2020) 106541

Contents lists available at ScienceDirect

Quaternary Science Reviews

journal homepage: www.elsevier.com/locate/quascirev

Invited paper

^{14}C and ^{10}Be dated Late Holocene fluctuations of Patagonian glaciers in Torres del Paine (Chile, 51°S) and connections to Antarctic climate change

Juan-Luis García [a, *], Brenda L. Hall [b], Michael R. Kaplan [c], Gabriel A. Gómez [a], Ricardo De Pol-Holz [d], Víctor J. García [e], Joerg M. Schaefer [c, f], Roseanne Schwartz [c]

[a] Instituto de Geografía, Pontificia Universidad Católica de Chile, Avenida Vicuña Mackenna 4860, Comuna Macul, Santiago, 782-0436, Chile
[b] School of Earth and Climate Sciences and Climate Change Institute, University of Maine, Orono, ME, 04469, USA
[c] Geochemistry, Lamont-Doherty Earth Observatory of Columbia University, Palisades, NY, 10964, USA
[d] Centro de Investigación GAIA-Antártica (CIGA) and Network for Extreme Environment Reasearch (NEXER), Universidad de Magallanes, Punta Arenas, Chile
[e] Espoz 4100, Dept. 32, Vitacura, Santiago, Chile
[f] Department of Earth and Environmental Sciences, Columbia University, New York, NY, 10027, USA

A R T I C L E I N F O

Article history:
Received 26 January 2020
Received in revised form
31 July 2020
Accepted 7 August 2020
Available online 30 August 2020

Keywords:
Torres del paine
Patagonian glaciers
Southern westerly winds
Holocene
Antarctic peninsula
Radiocarbon and ^{10}Be cosmogenic Dating

A B S T R A C T

Southern Hemisphere Holocene glacier chronologies are important for unraveling past climate change, mid-to-high latitude teleconnections, and regional to global climate forcing. At present, a significant number of glacier chronologies for Patagonia are based on ^{14}C dating, which may afford only maximum- or minimum-limiting dates. Here, we combine geomorphology and stratigraphy with radiocarbon (^{14}C) and beryllium-10 (^{10}Be) surface exposure-age dating at three outlet glaciers, Zapata, Tyndall, and Pingo. These glaciers drain the southernmost tip of the Southern Patagonian Ice Field at Torres del Paine National Park, Chile (51°S). After an expansion that we date at 3200 yr. B.P., the Torres del Paine glaciers expanded to their last major Late Holocene maxima at 600 and 340 yr. B.P., with the final dated readvance after 190 yr. B.P. We use these data, together with other Patagonian glacier records, to define the early, mid and final glacial stages of the last millennium. These cold events were separated by warm conditions that allowed the *Nothofagus* forest to colonize deglaciated land. The presence of near-concurrent glacier fluctuations in Patagonia and Antarctic Peninsula indicates widespread cooling punctuated the Late Holocene, including the last millennium, across much of the extratropical Southern Hemisphere. We link this cooling to cold oceanographic-atmospheric conditions forced by a northern shift or intensification of the Southern Westerly Winds. Such scenario increased northward advection of cold Antarctic circumpolar water along western Patagonia and favored decreased upwelling of warm circumpolar deep water together with expanded sea ice around the Antarctic Peninsula.

© 2020 Elsevier Ltd. All rights reserved.

1. Introduction

Mapping and geochronologic analysis of the Holocene glacial record afford a means of reconstructing past climate changes and associated driving mechanisms in the southern extratropical region (Strelin et al., 2014; Aniya, 2013a, b; Putnam et al., 2012; Schaefer et al., 2009; Mercer, 1965, 1968; Hall et al., 2019; Davies et al., 2020). Recent work has filled important gaps of the Holocene glacier history of southernmost south America, but more data are needed to unravel the footprint of climate variability within the southern mid-to-high latitudes (Kaplan et al., 2016; Reynhout et al., 2019; Hall et al., 2019). Glacially polished rock and unweathered moraine ridges document Holocene expansions of the South Patagonian Ice Field (SPIF) (Glasser et al., 2005; Marden and Clapperton, 1995; Davies et al., 2020), but most prior dating efforts have been restricted to maximum- or minimum-limiting radiocarbon (^{14}C) ages that do not always constrain the timing or extent of glaciation closely (Marden and Clapperton, 1995; Luckman and Villalba, 2001; Porter, 2000; Masiokas et al., 2009). This has in some cases limited the dating accuracy of glacial reconstructions and reduced their full usefulness as a proxy of climate

* Corresponding author.
E-mail address: jgarciab@uc.cl (J.-L. García).

https://doi.org/10.1016/j.quascirev.2020.106541
0277-3791/© 2020 Elsevier Ltd. All rights reserved.

change. Moreover, ^{14}C to calendar year calibration curves include periods of relatively high age uncertainties in the Late Holocene, in part due to global ^{14}C variations (Stuiver, 1978; Stuiver and Pearson, 1993).

To minimize these potential issues, we combine a detailed geomorphic and stratigraphic description with a composite radiocarbon (^{14}C) and beryllium-10 (^{10}Be) chronology to unravel the timing of Late Holocene (after 4200 yr. BP, in the sense of Walker et al., 2012) glacial fluctuations in Torres del Paine National Park, southern Chile (51°S; Fig. 1), with particular emphasis on the last major glacier expansion(s) (i.e., the last millennium). We focus our efforts on the southern outlet glaciers of the SPIF, with particular attention on Zapata Glacier, but also neighboring Pingo and Tyndall Glaciers (García et al., 2014). Use of multiple sites allowed us to find more ^{14}C dateable material and constrain spatial patterns in Holocene glacial and climate fluctuations along the southern margin of the SPIF. We then compare our results with existing chronologies of glacier change for Patagonia and the Antarctic Peninsula and elaborate on the possible atmospheric, oceanographic, and cryospheric teleconnections and climate mechanisms driving the Late Holocene ice fluctuations.

Exploring the geographic extent and linkage of glacial events between the middle and high latitudes of the Southern Hemisphere permits us to assess the possible role of the Southern Westerlies Winds (SWW) and the Southern Ocean in driving climate change during the Holocene (Clapperton and Sugden, 1988; Kaplan et al., 2020). The variability of Southern Ocean temperatures and the strength of the advection of cold waters from high to lower latitudes together with to the position of the SWW core is thought to play an important role in climate fluctuations within the last glacial period and its termination, but the behavior during the Holocene climate is less well-known (cf., Kilian and Lamy, 2012). Stadial conditions recorded in Antarctica and in the Southern Ocean correspond well with mid-latitude sea surface temperatures (SST) depressions and southern hemisphere glacier advances, revealing a close link during glacial periods (Lamy et al., 2004; García et al., 2012). At least during the 20th/21st century the Southern Annular Mode (SAM) is associated with converging air temperature but opposite precipitation trends between the southern mid and high latitudes (Garreaud, 2007; Garreaud et al., 2013). In the context of the last decades, when major glacier retreat in Patagonia and the Antarctic Peninsula generally occurred, we aim to understand possible the paleoatmosphere-ocean patterns that may have also linked both regions during the Late Holocene.

2. Study area and setting

Pingo, Zapata and Tyndall Glaciers drain the southeast margin of the SPIF (Fig. 1). Whereas Pingo and Tyndall Glaciers flow predominantly south-southeast and today terminate in prominent lakes dammed by moraines, the northern and southern Zapata Glaciers diverge from Tyndall Glacier and end on recently deglaciated, well-polished shale bedrock (Aniya and Sato, 1995a). The lakes are relatively recent features; when the moraines formed, Pingo and Tyndall Glaciers were land terminating. The climate in this region is influenced strongly by maritime air masses transported by the SWW across the Pacific Ocean. Mean annual temperature reaches 6 °C in the surrounding lower areas. The SWW transport moisture-bearing storm systems that bring abundant frozen precipitation to the ice field throughout the year. Even though the southern Andes are <2000 m a.s.l., the orographic effect produces more than 8 m/year of precipitation at the SPIF divide (Schneider et al., 2003). The mid-latitude setting, along with high precipitation rates and a substantial long summer ablation season given temperatures around and above 0 °C, leads to high mass balance gradients and a high throughput, and thereby outlet glaciers that are particularly sensitive to climate fluctuations (Mackintosh et al., 2017; Davies et al., 2020). In Patagonia, specifically, observations from the 20th and 21st centuries document that summer temperature has a significant effect on regional mass balance on timescales of decades or longer (Kerr and Sugden, 1994; Rivera and Casassa, 2004; Rignot et al., 2003; Oerlemans, 2005; Sagredo et al., 2014; Barcaza et al., 2017).

In the study area, Middle and Late Holocene glacier fluctuations are well represented by widespread moraine belts fringing the SPIF (Röthlisberger, 1986; Masiokas et al., 2009; Strelin et al., 2014; Kaplan et al., 2016; Davies et al., 2020). Prior to the formation of Late Holocene glacier limits, which are the focus of this study (Fig. 1), ice retreated from the Late Glacial frontal limits (García et al., 2012) at the eastern end of Torres del Paine National Park, around 13 kyr B.P. or soon after (Moreno et al., 2009). The next inboard set of moraines just east of the Zapata/Pingo/Tyndall area occurs around the southern end of Lago Grey near Lago Margarita (Marden and Clapperton, 1995). These features are assumed to be Middle Holocene in age (>3810 ± 85 yr. B.P yr.) based on minimum-limiting ^{14}C ages from a peat core (Moreno et al., 2009), but direct dating is lacking. Latest Holocene extents of the outlet glaciers were confined to the area shown on Fig. 1B. We mapped two distinct ice marginal positions at Zapata Glacier, which also seem to occur at Pingo and Tyndall Glaciers. These two moraines belts in some cases are separated by different generations (i.e., morphostratigraphic settings) of outwash plains (Pingo) or by rivers (Tyndall) (Fig. 1). We follow Marden and Clapperton (1995) and recent work in the Torres del Paine region (García et al., 2012, 2014) in naming these moraine belts TDP VI (outer) and TDP VII (inner).

The Holocene moraine sequences in different valleys within Torres del Paine National Park were mapped previously by Röthlisberger (1986), Marden and Clapperton (1995) and Aniya and Sato (1995a). Röthlisberger (1986) provided a maximum age range of 680–185 yr. B.P. for the deposition of the inner moraines at Francés and Perro Glaciers. By applying a tree-ring chronologic approach at the Grey Glacier, Marden and Clapperton (1995) estimated the inner TDP VII ridges (their H moraine) to be deposited during the 17th-20th centuries. In contrast, Aniya and Sato (1995a), using minimum- (basal sediments from bogs) and maximum- (wood embedded in glacial sediment) limiting ^{14}C dates, interpreted the TDP VII moraine landforms deposited by the Zapata Glacier as representing four main advances ranging from ca. 3800 to 300 yr. B.P. In this paper, we expand the chronology at Zapata Glacier, and discuss the paleoclimate implications of the combined record from Zapata, Pingo, and Tyndall Glaciers.

3. Materials and methods

We mapped the geomorphology of the region using a stereoscope over printed panchromatic aerial photograph pairs (1:70.000, Servicio Aerofotogramétrico de Chile), which were checked in the field during several campaigns between 2009 and 2014. In the field, we analyzed glacial sediments cropping out in stratigraphic sections that record local ice fluctuations. We hand-sampled the outer layers of well-preserved tree trunks and twigs within glacial sediments cropping out in moraine ridges for ^{14}C dating. No bark was preserved and samples ages should correspond to the youngest part dated of one piece of wood at the site. These organic materials are interpreted as remains incorporated when ice advanced over a forest. We also collected ^{14}C samples from the

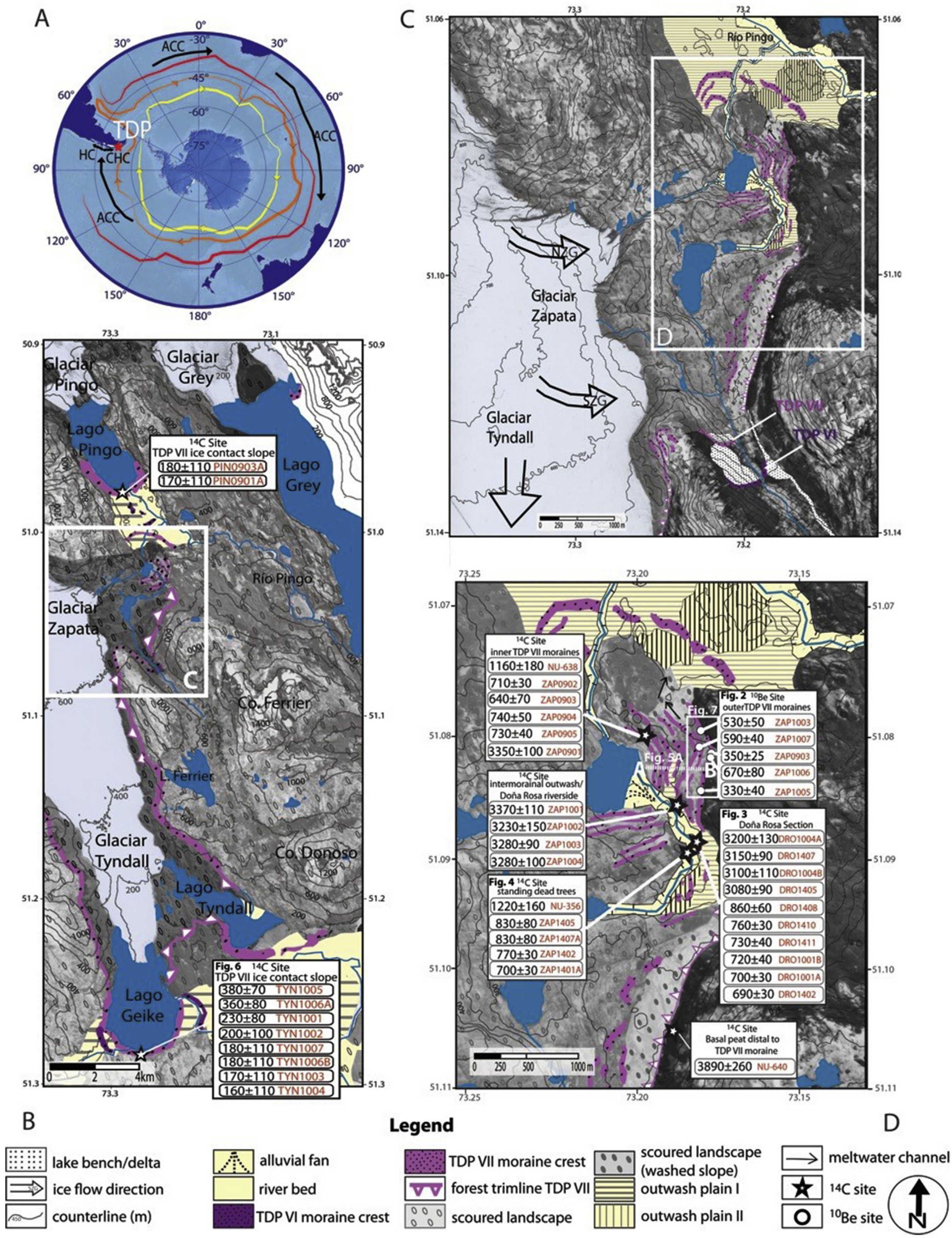
A
ACC
TDP
HC
CHC
C
Río Pingo
Glaciar Zapata
Glaciar Tyndall
NZG
SZG
D
TDP VII
TDP VI
Glaciar Pingo
Glaciar Grey
Lago Pingo
Lago Grey
14C Site
TDP VII ice contact slope
180±110 PIN0903A
170±110 PIN0901A
Río Pingo
Glaciar Zapata
Co. Ferrier
L. Ferrier
Glaciar Tyndall
Co. Donoso
Lago Tyndall
Lago Geike
Fig. 6 14C Site
TDP VII ice contact slope
380±70 TYN1005
360±80 TYN1006A
230±80 TYN1001
200±100 TYN1002
180±110 TYN1007
180±110 TYN1006B
170±110 TYN1003
160±110 TYN1004
B
14C Site
inner TDP VII moraines
1160±180 NU-638
710±30 ZAP0902
640±70 ZAP0903
740±50 ZAP0904
730±40 ZAP0905
3350±100 ZAP0901
14C Site
intermorainal outwash/
Doña Rosa riverside
3370±110 ZAP1001
3230±150 ZAP1002
3280±90 ZAP1003
3280±100 ZAP1004
Fig. 4 14C Site
standing dead trees
1220±160 NU-356
830±80 ZAP1405
830±80 ZAP1407A
770±30 ZAP1402
700±30 ZAP1401A
Fig. 2 10Be Site
outerTDP VII moraines
530±50 ZAP1003
590±40 ZAP1007
350±25 ZAP0903
670±80 ZAP1006
330±40 ZAP1005
Fig. 7
Fig. 5A
A
B
Fig. 3 14C Site
Doña Rosa Section
3200±130 DRO1004A
3150±90 DRO1407
3100±110 DRO1004B
3080±90 DRO1405
860±60 DRO1408
760±30 DRO1410
730±40 DRO1411
720±40 DRO1001B
700±30 DRO1001A
690±30 DRO1402
14C Site
Basal peat distal to
TDP VII moraine
3890±260 NU-640
D
Legend
lake bench/delta
ice flow direction
counterline (m)
alluvial fan
river bed
TDP VI moraine crest
TDP VII moraine crest
forest trimline TDP VII
scoured landscape
scoured landscape (washed slope)
outwash plain I
outwash plain II
meltwater channel
14C site
10Be site
N

outer layers of exhumed, dead, standing trees (i.e., in life-position), which were buried in proglacial glaciofluvial sediments during a glacial advance. Some of these tree stumps were located at the present river bed (Aniya and Sato, 1995a). We produced probability plots of ^{14}C ages of wood obtained from till sections and moraines to look for distinct populations within the dataset that can be related to glacial advances. This approach allows us to consider the inherent scatter of ^{14}C analyses more precisely than by using the single youngest age approach (Luckman and Villalba, 2001), which in some cases could be affected by laboratory pretreatment or measurement error. In other cases, scatter may also contain information on the duration of the warm period, as discussed below. All ^{14}C ages presented in this paper ($n = 33 +$ six ages from Aniya and Sato, 1995a; Table 1) were calibrated to calendar years using the SHcal13 curve (Hogg et al., 2013) and are rounded to the closest decade. We report calibrated ^{14}C ages using the 2-sigma range of the maximum probability, except in Fig. 8 and 9, where we show calibrated ^{14}C date ± 1 sigma.

To constrain the age of the Late Holocene moraines directly, we sampled boulders for ^{10}Be cosmogenic exposure dating from the outer TDP VII ridges deposited by the Zapata Glacier (Fig. 1). We followed standard protocols for sampling and processing as described in Schaefer et al. (2009) and Kaplan et al. (2016). All elevations were measured with a hand-held GPS. We used the Patagonian ^{10}Be production rate derived in the nearby Lago Argentino basin (Kaplan et al., 2011), and version 3 of the online calculator (Balco et al., 2008) (Table 2) to calculate exposure dates. For direct comparison, both the ^{14}C and the ^{10}Be ages are referred to as years before present (B.P., AD 1950), and 60 years were subtracted from the latter (Table 3), given the years of sampling (2009 and 2010).

4. Results

4.1. Zapata Glacier

The Zapata Glacier includes two sub-lobes: northern Zapata Glacier (NZG) and southern Zapata Glacier (SZG) (Fig. 1). The TDP VI and VII moraine belts are separated by ~1.3 km at the SZG. However, at the NZG only the TDP VII moraine was mapped, as the TDP VI moraine could not be distinguished, perhaps because of dense *Nothofagus* forest. At the SZG, a 300 m wide flat TDP VI landform is preserved on both sides of the valley, about 4 km from the present ice field (Aniya and Sato, 1995a, Fig. 1). We interpret this landform to be an ice-contact delta. A continuous lacustrine bench at ~600 m a.s.l. is stratigraphically related to this TDP VI landform (Aniya and Sato, 1995a). At the SZG we also mapped a local sequence of lake benches and shorelines at and below ~500 m a.s.l. formed after ice left the TDP VI margin. Of the studied glaciers, the SZG is the only glacier to have terminated in a glacial lake during moraine formation. We infer that the other glaciers ended on land as based on geomorphic observations. For instance, the frontal moraines at Pingo grade to an outwash plain; the same is true for the moraine outlining Lago Tyndall. The NZG and the Tyndall Glacier (Lago Geike basin) buttressed against mountain relief.

At NZG, the TDP VII moraines consist of 10–15, mostly unvegetated, sharp ridges deposited on steep, frost- shattered shale bedrock. Moraines have incorporated reworked wood and ice-abraded quartz-bearing boulders, suitable for ^{14}C and ^{10}Be dating, respectively. A distinct, narrow outwash plain separates outer and inner TDP VII ridges. A continuous well-defined moraine and a sharp boundary in forest vegetation type and age marks the outer ridge of the TDP VII limit (Fig. 2C). Sections of this outer moraine consist of grouped boulders, with no fine matrix (Fig. 2 D and E). We sampled boulders from the outer ridges of the TDP VII belt of the NZG for ^{10}Be dating.

4.1.1. Radiocarbon dating

We collected 33 wood samples associated with the TDP VII moraines from three settings: (1) within till and outwash cropping out in multiple TDP VII ridges (51.085°S; 73.272°W; 51.090°S; 73.267°W) (Fig. 1B and D), (2) within a stratigraphic section by Río Doña Rosa (51.094°S; 73.263°W) (Fig. 3A), and (3) from standing, dead *Nothofagus* stumps unburied from glacial outwash (51.094°S; 73.265°W) (Fig. 4). Five samples came from within the TDP VII innermost ridges deposited by the NZG. Four of these were small reworked wood pieces (samples ZAP0902 – ZAP0905) cropping out on the surface of moraines. Their ages ranged between 640 ± 50 and 740 ± 70 yr. B.P. with a mean of 705 ± 45 yr. B.P. The remaining fifth sample, a small wood piece embedded in till from the TDP VII innermost crest, produced a distinctly different age of 3350 ± 100 yr. B.P. (ZAP0901, Table 1).

Within the TDP VII extent of the NZG, the Río Doña Rosa incised different generations of glacial sediments and exposed a ~25 m section at the eastern canyon wall (Figs. 1 and 3). Three main units occur from close to the present riverbank to the top of the section, where either TDP VII moraine or outwash occur. The lowermost unit is a massive to coarsely bedded, clast-rich diamicton, including sub-angular cobbles embedded within an indurated silty matrix, which we interpret as a traction till (Evans et al., 2006, Fig. 3B). Well-laminated glaciolacustrine sediments, including mud to gravel grain sizes, are intercalated with the till. Four wood samples (DRO1004A and B, DRO1405 and DRO1407) within the till yielded ages between 3200 ± 130 and 3080 ± 90 yr. B.P., with a mean of 3130 ± 50 yr. B.P. (Table 1). A few tens of meters to the north, three wood samples (ZAP1001, ZAP1002 and ZAP1003) were sampled from the intermorainal TDPVII outwash plain surface and from a till unit in the canyon wall and yielded a similar age range between 3370 ± 110 yr. B.P. and 3280 ± 90 yr. B.P. Fig. 3B shows the till is overlain unconformably by parallel, cross-laminated, gravelly and silty sand, which we interpret as distal outwash sediments. Abundant transported twigs and wood fiber occur at the base of this unit on the lower unconformity surface, from where we obtained an age of 860 ± 60 yr. B.P. (DRO1408). The grain size increases upward into the third unit, a massive to coarsely bedded, matrix-to-clast-supported angular to subangular gravelly diamicton. The contact surface with the underlying cross-bedded sediment unit is unconformable and erosive. Sand lenses highlight crude bedding, which we interpret as debris flows at the ice margin linked to the moraine built at the top of the section. The ages of five wood

Fig. 1. Geomorphologic map of Pingo, Zapata and Tyndall Glacier basins in Torres del Paine National Park (Chile). A. Polar projection showing the location of Torres del Paine (TDP, red star) in southernmost South America within the Antarctic and Southern Ocean geographic context. Colored lines represent approximate location of ocean fronts (red: Subtropical Front; orange: Sub-Antarctic Front; yellow: Polar Front; ACC: Antarctic Circumpolar Current; CHC: Cape Horn Current; HC: Humboldt Current. **B.** Study area including new ^{14}C data obtained from TDP VII moraines at Pingo and Tyndall Glaciers. **C.** Zoom into the Zapata Glacier area, where it is possible to distinguish the southern Zapata Glacier (SZG) and the northern Zapata Glacier (NZG). The map depicts the erosional and depositional features, including the Mid to Late Holocene TDP VI and TDP VII moraine belts. **D.** Detailed map with the geochronologic record obtained in this study at the NZG. White boxes in all maps display ^{14}C calibrated ages (star symbol on map; 2 sigma errors) and ^{10}Be ages (white circles; 1 sigma error). The ^{14}C ages provide evidence for times when outlet glaciers of the Southern Patagonian Ice Field at Torres del Paine advanced, overriding *Nothofagus* forest. The ^{10}Be ages document the culmination of two glacial advances that ended with the construction of the TDP VII moraine complex (see text for details). The A-B transect (white dashed line) across the NZG moraines in **D** shows the location of the topographic profile displayed in Fig. 5a. (For interpretation of the references to colour in this figure legend, the reader is referred to the Web version of this article.)

Table 1
Radiocarbon data obtained from wood in glacial sediments and landforms at Zapata, Tyndall and Pingo Glaciers, Torres del Paine National Park, south Chile. For site location see Fig. 1. See the text for latitude and longitude coordinates.[a]

Sample Id	Lab Code	^{14}C age (yr. B.P.)	Error 1σ (yr. B.P.)	2σ calendar range age (yr. B.P.)	Mean calendar age (yr. B.P.)	Error 2σ (yr. B.P.)	Context
ZAP1001	OS-81261	3210	35	3255–3476	3370	110	Down river Doña Rosa stratigraphic section: wood in lower till, northern Zapata Glacier
ZAP0901	OS-81260	3190	30	3252–3450	3350	100	Wood in innermost TDP VII moraine ice-contact slope, northern Zapata Glacier
ZAP1002	OS-81262	3100	40	3084–3377	3230	150	Down river Doña Rosa stratigraphic section: wood in lower till, northern Zapata Glacier
ZAP1003	OS-81263	3120	25	3184–3372	3280	90	Down river Doña Rosa stratigraphic section: wood in lower till, northern Zapata Glacier
ZAP1004	OS-81264	3120	30	3182–3376	3280	100	Wood exposed in intermorainal TDP VII outwash, northern Zapata Glacier
DRO1004A	UCIAMS-89031	3040	20	3073–3324	3200	130	Doña Rosa stratigraphic section: wood in lower till, northern Zapata Glacier
DRO1407	UCIAMS-145274	3025	15	3065–3235	3150	90	Doña Rosa stratigraphic section: wood in lower till, northern Zapata Glacier
DRO1004B	UCIAMS-89032	2985	20	2994–3206	3100	110	Doña Rosa stratigraphic section: wood in lower till, northern Zapata Glacier
DRO1405	UCIAMS-145273	2975	15	2990–3169	3080	90	Doña Rosa stratigraphic section: wood in lower till, northern Zapata Glacier
DRO1408	UCIAMS-145275	995	15	802–920	860	60	Doña Rosa stratigraphic section: wood within stratified deltaic sandy organic sediment, northern Zapata Glacier
ZAP1405	UCIAMS-145270	950	15	750–904	830	80	Standing dead tree within glaciofluvial sandy gravel at Río Doña Rosa, northern Zapata Glacier
ZAP1407A	UCIAMS-145271	950	15	750–904	830	80	Standing dead tree within glaciofluvial sandy gravel at Río Doña Rosa, northern Zapata Glacier
ZAP1402	UCIAMS-145269	920	15	736–799	770	30	Standing dead tree within glaciofluvial sandy gravel at Río Doña Rosa, northern Zapata Glacier
DRO1410	UCIAMS-145276	890	15	726–788	760	30	Doña Rosa stratigraphic section: wood in upper flow till, northern Zapata Glacier
ZAP0904	UCIAMS-89035	880	20	687–788	740	50	Wood embedded in inner TDP VII moraines, northern Zapata Glacier
ZAP0905	UCIAMS-89036	865	20	684–766	730	40	Wood embedded in inner TDP VII moraines, northern Zapata Glacier
DRO1411	UCIAMS-145277	870	15	685–768	730	40	Doña Rosa stratigraphic section: wood in upper flow till, northern Zapata Glacier
DRO1001B	UCIAMS-89030	855	20	679–761	720	40	Doña Rosa stratigraphic section: wood in upper flow till, northern Zapata Glacier
ZAP0902	UCIAMS-89033	835	20	676–734	710	30	Wood embedded in inner TDP VII moraines, northern Zapata Glacier
DRO1001A	UCIAMS-89029	830	20	675–732	700	30	Doña Rosa stratigraphic section: wood in upper flow till unit, northern Zapata Glacier
ZAP1401A	UCIAMS-145268	805	15	669–722	700	30	Standing dead tree within glaciofluvial sandy gravel at Río Doña Rosa, northern Zapata Glacier
DRO1402	UCIAMS-145272	780	20	656–721	690	30	Doña Rosa stratigraphic section: wood in upper flow till, northern Zapata Glacier
ZAP0903	UCIAMS-89034	760	20	572–712	640	70	Wood embedded in inner TDP VII moraines, northern Zapata Glacier
TYN1005	UCIAMS-89026	350	20	309–451	380	70	Wood embedded in innermost TDP VII ice-contact slope, Tyndall Glacier
TYN1006A	UCIAMS-89027	305	20	288–440	360	80	Wood embedded in innermost TDP VII ice-contact slope, Tyndall Glacier
TYN1001	OS-81265	235	30	143–309	230	80	Wood embedded in innermost TDP VII ice-contact slope, Tyndall Glacier
TYN1002	OS-81266	210	25	105–297	200	100	Wood embedded in innermost TDP VII ice-contact slope, Tyndall Glacier
TYN1006B	UCIAMS-89028	190	20	67–283	180	110	Wood embedded in innermost TDP VII ice-contact slope, Tyndall Glacier
TYN1007	OS-81268	210	25	71–297	180	110	Wood in glaciofluvial sediment distal to TDP VII moraine, Tyndall Glacier
PIN0903A	UCIAMS-89023	195	20	71–284	180	110	Wood embedded in innermost TDP VII ice-contact slope, Pingo Glacier
TYN1003	OS-81267	175	25	56–280	170	110	Wood embedded in innermost TDP VII ice-contact slope, Tyndall Glacier
PIN0901A	UCIAMS-89024	185	20	59–281	170	110	Wood embedded in innermost TDP VII ice-contact slope, Pingo Glacier
TYN1004	UCIAMS-89025	150	20	52–264	160	110	Wood embedded in innermost TDP VII ice-contact slope, Tyndall Glacier
_	NU-640	3630	95	3635–4153	3890	260	Basal peat sample distal to TDP VII outer moraine, southern Zapata Glacier
_	NU-356	1370	80	1060–1371	1220	160	Standing dead tree in glaciofluvial sandy gravel at Río Doña Rosa, northern Zapata Glacier
_	NU-638	1330	80	985–1342	1160	180	Wood embedded in inner TDP VII moraines, northern Zapata Glacier

(continued on next page)

Table 1 (*continued*)

Sample Id	Lab Code	^{14}C age (yr. B.P.)	Error 1σ (yr. B.P.)	2σ calendar range age (yr. B.P.)	Mean calendar age (yr. B.P.)	Error 2σ (yr. B.P.)	Context
_	NU-639	980	120	652–1088	870	220	Wood obtained from a pit dug in the outermost TDP VI moraine, southern Zapata Glacier
_	NU-636	950	110	656–1055	860	200	Wood embedded in inner TDP VII moraine, southern Zapata Glacier
_	NU-637	290	–	146–462	300	160	Basal peat sample proximal to TDP VII moraine, southern Zapata Glacier

[a] NU samples at bottom of table from Aniya and Sato (1995a).

Table 2
Glacier Zapata TDP VII outer moraine ^{10}Be sample attributes and data.

CAMS laboratory no.	Sample ID	Latitude (decimal degree)	Longitude (decimal degree)	Elevation (m a.s.l.)	Boulder size (L x W x H) (cm)	Sample thickness (cm)	Shielding correction	Quartz weight (g)	Carrier Added (g)[a]	^{10}Be/^{9}Be ± 1σ (10^-14)[b]	[^{10}Be] ± 1σ (10^3 atoms × g^{-1})	AMS Standard[c]
BE30287	ZAP0903	−51.0860	−73.2609	356	630 x 480 x 310	0.90	0.9977	46.6601	0.1606	1.130E ± 0.085E	2.4280 ± 0.1852	07KNSTD
BE30288	ZAP1003	−51.0854	−73.2609	350	300 x 200 x 290	1.50	0.9961	38.3565	0.1601	1.317E ± 0.120E	3.4784 ± 0.3170	07KNSTD
BE30289	ZAP1005	−51.0869	−73.2599	362	280 x 210 x 190	0.90	0.9902	26.3625	0.1396	0.757E ± 0.092E	2.3291 ± 0.2874	07KNSTD
BE30290	ZAP1006	−51.0862	−73.2610	363	170 x 110 x 115	1.60	0.9966	36.4312	0.1391	1.773E ± 0.206E	4.3327 ± 0.5039	07KNSTD
BE30291	ZAP1007	−51.0857	−73.2620	318	210 x 110 x 150	0.90	0.9902	29.4689	0.1396	1.258E ± 0.082E	3.7082 ± 0.2460	07KNSTD
	Blank_1_2010Aug31								0.1612	0.110E ± 0.031E		07KNSTD
	Blank_2_2010Aug31								0.1602	0.088E ± 0.025E		07KNSTD

[a] Samples were measured with a Be carrier concentration of 996 ppm.
[b] ^{10}Be/^{9}Be values have been corrected for background ^{10}Be concentrations (atoms/g) detected in procedural blanks.
[c] Reported ^{10}Be/^{9}Be value for 07KNSTD is 2.85×10^{-12} (Nishiizumi et al., 2007). Density of rock used for calculating ^{10}Be ages is 2.65 g cm^{-3}.

Table 3
^{10}Be ages in years ago and before present (1950) for the Glacier Zapata TDP VII outer moraine.[a]

Sample ID	St		Lm		LSDn	
	year ago	year B.P.	year ago	year B.P.	year ago	year B.P.
ZAP0903	**410 ± 30**	**350 ± 25**	440 ± 35	380 ± 30	450 ± 35	390 ± 30
ZAP1003	**590 ± 55**	**530 ± 50**	620 ± 60	560 ± 50	630 ± 55	570 ± 50
ZAP1005	**390 ± 50**	**330 ± 40**	420 ± 50	360 ± 45	440 ± 55	380 ± 45
ZAP1006	**730 ± 85**	**670 ± 80**	760 ± 90	700 ± 80	750 ± 85	690 ± 80
ZAP1007	**650 ± 45**	**590 ± 40**	680 ± 45	620 ± 40	680 ± 45	620 ± 40

[a] ^{10}Be ages ± internal or analytical error (1σ, AMS). ^{10}Be ages shown as reported by the online exposure age calculator v.3 (Balco et al., 2008): "St" is the is the time dependent scaling scheme of Stone (2000); "Lm" is the time dependent version of Stone/Lal scaling scheme (Lal, 1991; Stone, 2000); LSDn is the time dependent version of Lifton et al. (2014) scaling scheme. We use the "St" scaling scheme but this choice does not change our conclusions. All ages were calculated using a ^{10}Be production rate measured at Lago Argentino, south Patagonia (50°S) (Kaplan et al., 2011).

samples (DRO1001A, DRO1001B, DRO1402, DRO1410 and DRO1411) embedded within this upper diamicton ranged between 760 ± 30 and 690 ± 30 yr. B.P., yielding a mean of 720 ± 30 yr. B.P. (Table 1; Fig. 3B and C).

Many dead tree trunks (1–3 m tall) standing in life position occur in both the riverbed and the riverbank at the bottom of Río Doña Rosa canyon, as previously found by Aniya and Sato (1995a). They were buried and killed by glaciofluvial sediment as ice approached, and therefore their ^{14}C ages are linked to advances of the NZG. New radiocarbon dates obtained from four different specimens ranged between 830 ± 80 and 700 ± 30 yr B.P., yielding a mean of 780 ± 60 (ZAP1401A, ZAP1402, ZAP1405, ZAP1407A, Fig. 4), younger than a date reported previously of 1220 ± 160 yr. B.P. by Aniya and Sato (1995a, NU-356) (Table 1).

4.1.2. ^{10}Be dating

Data from five ^{10}Be samples obtained from the TDP VII outer ridges of the NZG are shown in Table 2. In the field, we sampled two main outer crests within the TDP VII moraine belt: Samples ZAP0903, ZAP1003, ZAP1005 and ZAP1006 were recovered at the forest trimline, and ZAP1007 was collected from an inboard ridge. All sampled boulders rested in apparently stable positions and lacked obvious signs of erosion or weathering. Ages ranged from 670 ± 80 yr. B.P. to 330 ± 40 yr. B.P. (Table 3), with a bimodal distribution (Fig. 5B). The older group of ages average to 600 ± 70 yr. B.P. (1σ range; n = 3; ZAP1003, ZAP1006, ZAP1007) and the younger group average to 340 ± 20 yr. B.P. (1σ range; n = 2; ZAP0903, ZAP1005). In each part of the bimodal distribution, the respective ages overlap at 1-2σ. Boulders sampled at the trimline include both modes of ages. As discussed below, it is not clear why this is so, as there is no obvious relationship between age and location; indeed, one of the oldest ages is on an inboard ridge (ZAP1007).

4.2. Tyndall Glacier

The TDP VI and TDP VII moraines enclose Lago Geike, where surrounding topography constrained the former ice extent (Fig. 1B). These moraines have as much as 50 m of relief. The TDP VI moraine is well preserved to the southeast and east of Lago Geike and supports a mature *Nothofagus* forest, with trees growing on top of boulders. The TDP VII moraine is prominent and follows the shore of Lago Geike (Fig. 1B). This ice limit corresponds stratigraphically with the forest trimline stretching towards the Zapata Glacier area to the north. Wave action has eroded and steepened the original ice-contact slope. This erosion has exposed wood protruding from the till that makes up the TDP VII moraine. The TDP VII moraine grades south into an outwash plain that separates it from the southwards TDP VI moraine by as much 500 m.

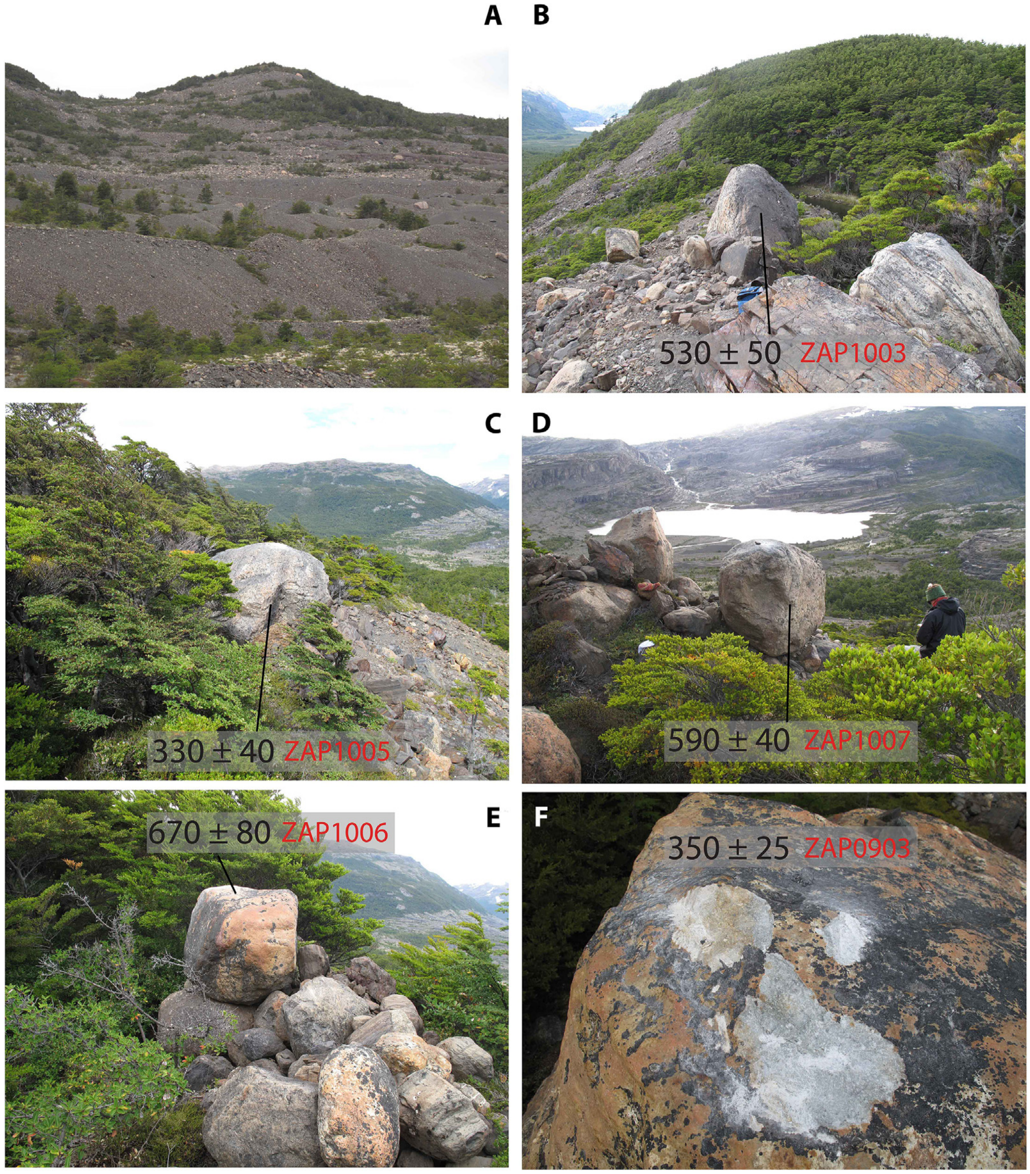

Fig. 2. Moraines and boulders sampled for ^{10}Be cosmogenic dating at Zapata Glacier. A. TDP VII moraine belt deposited by the northern Zapata Glacier. Here, a total of 10–15 well-preserved moraine ridges deposited over a step-wise rock relief comprise the TDP VII landform. **B–F,** sampled boulders from the outer moraine ridges of TDP VII belt analyzed for ^{10}Be dating. Ages display 1 sigma analytical error only. Note the forest trimline in **B**, **C** and **E** indicates the maximum extent of the Southern Patagonian Ice Field during the last millennium in Torres del Paine. Photo in **D** points toward the ice field (west) and exposes the relatively recent deglaciated well-polished shale bedrock in the background. In 1944 AD the Zapata Glacier front was just inboard of the lake in the picture.

4.2.1. *Radiocarbon dating*

We collected eight wood samples (TYN-, Table 1) from ripped up tree trunks, branches and twigs protruding from the ice-contact slope of the TDP VII moraine adjacent to Lago Geike (51.315°S; 73.267°W) (Fig. 1B). The ages ranged from 160 ± 110 to 380 ± 70 yr. B.P. with a mean of 230 ± 90 yr. B.P. (Fig. 6). We also obtained an age of 200 ± 100 yr. B.P. (TYN1002) from a reworked wood sample from sandy gravelly outwash exposed in a section distal to TDP VII moraine.

4.3. *Pingo Glacier*

The outer TDP VI position at Pingo Glacier is only recorded by patchy landforms that lack evidence of a clear ice limit, because the area between Lago Pingo and Zapata Glacier consist of an extensive outwash plain. This outwash plain can be tracked to the TDP VII moraine that encloses Lago Pingo. Two to three ridges comprise the TDP VII moraine belt here. These ridges are 2–5 m tall with slopes close to the angle of repose (~30°), except at the shoreline, where active wave erosion has produced a steeper ice-contact slope. These inner TDP VII moraines are partially covered by small *Nothofagus* trees.

4.3.1. *Radiocarbon dating*

Two samples (Table 1, Fig. 1) from a single wood fragment embedded within the indurated sediment making up the inner-most ice-contact slope of the TDP VII moraine (51.051°S; 73.295°W) date to 180 ± 110 and 170 ± 110 yr. B.P. (PIN0901A and PIN0903A).

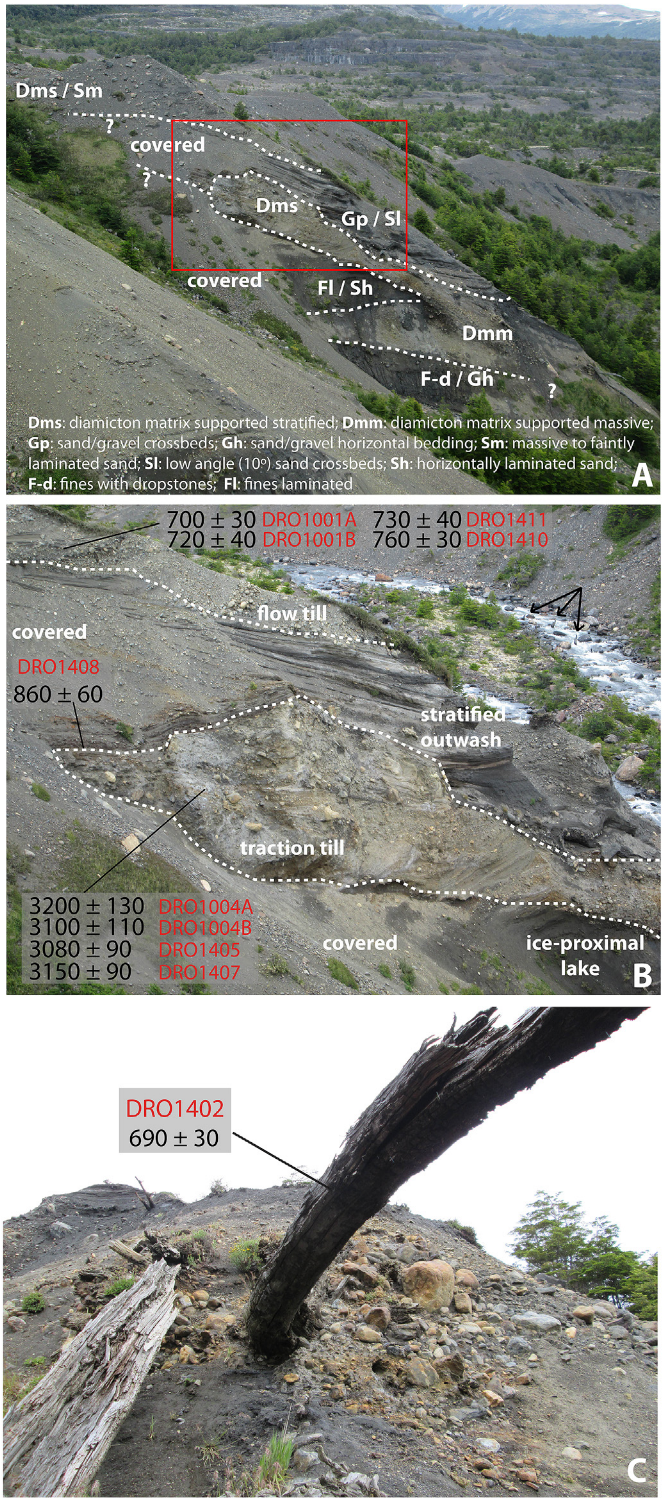

Fig. 3. Doña Rosa stratigraphic section on the eastern side of the Río Doña Rosa canyon, Zapata Glacier. A. Sediment lithofacies in Doña Rosa Stratigraphic section (modified from Eyles et al., 1983). **B.** Detail of the Doña Rosa stratigraphic section (red box in A), including interpretation of sediment facies, and calibrated radiocarbon ages of wood fragments embedded in glacial sediments (2 sigma error). In the background, the Río Doña Rosa and a number of dead standing trees (black arrows) can be seen within the river channel (Fig. 4). **C.** Mature-size tree trunks outcropping in till sediments at the Doña Rosa Stratigraphic section. The photo displays a calibrated radiocarbon age obtained from one of the exceptionally well-preserved logs that occur here, which provide a maximum age for the glacial advance represented by the till. (For interpretation of the references to colour in this figure legend, the reader is referred to the Web version of this article.)

5. Discussion

5.1. Glacial geomorphology

The TDP VI and VII moraines are the result of two distinct constructional episodes at the Zapata, Tyndall and Pingo Glaciers. This is based on the separation of the two moraines as mapped across the studied glaciers, although at the Pingo site the outer TDP VI moraine is preserved only as patchy landforms. The most convincing site for the existence of two distinct ice-marginal positions is at the SZG, where the outer TDP VI limit occurs as a vegetated ice-contact delta and the inner TDP VII limit as a composite group of mostly unvegetated ridges that can be tracked north towards the NZG site. South of Lago Geike, both TDP VII and VI moraines are also well preserved. Everywhere we mapped the TDP VI moraine, it occurs beyond the limit of TDP VII margin and represents a larger glacial expansion. It is possible that the Pingo and Zapata ice fronts merged during the TDP VI advance, but no definitive geomorphic clues are preserved. The forest trimline mapped between the Tyndall and Zapata Glaciers is continuous and suggests that the two glaciers expanded synchronously during TDP VII advance (Fig. 1).

Only the SZG terminated in an ice-dammed lake, as indicated by the TDP VI ice-contact delta and by the extensive lacustrine bench at ~600 m a.s.l. that occurs proximal and distal to this landform at the SZG. Similarly, well-developed lake shorelines at ~500 m a.s.l. and below this elevation, together with glaciolacustrine sediments at the Doña Rosa sediment section, indicate that glacial lakes also persisted at a lower elevation during the TDP VII advance. These lakes extended few kilometers from the ice and were confined by local topography. They developed between the SZG and Tyndall Glacier. The lakes did not affect the ^{10}Be-sampled boulders, which were deposited at the terrestrial TDP VII ice front of the NZG, >5 km to the south of mapped lake terraces. At this location, the NZG was buttressed against the bedrock relief.

5.2. Interpretation of dates

5.2.1. Radiocarbon

There are two types of wood that may be incorporated by a glacier during an advance - that previously dead and reworked from some reservoir and that killed by the advance itself (or possibly by the cold temperatures that preceded the advance) (cf., Hall et al., 2019). We assume that a well-defined peak in a summed probability plot represents the latter and affords a close-limiting maximum, or even an exact age for glacial advance or kill event, within uncertainty. The peak in the probability plot in this case is favored over the youngest sample as an age for the advance, because we assume that the (statistical) error around the mean age is due to non-geologic factors (e.g., lab error, calibration uncertainty, surface contamination). On the other hand, populations of ages with poorly defined peaks or bimodal distributions unrelated to calibration uncertainties likely reflect at least partial reworking of wood from some reservoir. In this case, the youngest date should be used to reflect a maximum age for the advance. In addition, we assume that the time-period between two well-defined probability peaks delimits the maximum potential length of time between advances when there may have been ice-free conditions suitable for forest growth.

We combine the radiocarbon data for all three sites (Zapata, Pingo and Tyndall) to constrain glacier response along the southern SPIF. Fig. 8 shows three distinct populations of ^{14}C dates on wood obtained in this study at all sites. Despite the fact that ^{14}C-dated wood comes from three different geologic settings (lodged in till,

Fig. 4. Exhumed dead-standing trees in life position at the Río Doña Rosa, Zapata Glacier. Radiocarbon calibrated ages represent the time when trees were drowned by glacial outwash. **A.** ^{14}C **s**amples ZAP1401a and ZAP1402 were obtained from logs at the eastern Río Doña Rosa bank. **B.** ^{14}C sample ZAP1407 obtained from a log at the Doña Rosa channel.

exposed in moraines and outwash, and in growth position within glaciofluvial sediments) and comprises different wood types (rooted trunks, sheared branches, loose twigs), the samples group in clusters that afford evidence for ice expanding over a *Nothofagus* forest (cf., Hall et al., 2019). We therefore regard our ^{14}C data as close-maximum ages for SPIF glacial expansions that occurred at or just after 3210 yr. B.P. (Zapata Glacier), 720 yr. B.P. (Zapata Glacier), and 190 yr. B.P. (Pingo and Tyndall Glaciers).

5.2.2. Beryllium-10

We interpret the cosmogenic dates obtained from boulders resting on or embedded on top of the outer TDP VII moraines ridges as the near-culmination of the glacial advance by the NZG. The bimodal distribution of the five ^{10}Be exposure ages suggests the data are the result of more than one ice expansion reaching the same ice extent; that is, all the samples do not come from a single glacier expansion. Four of the five samples were obtained at the forest trimline, interpreted to represent maximum ice extent during the TDP VII advance. The fifth sample (ZAP1007) was collected from a ridge inboard from the forest trimline (Fig. 7). Nevertheless, it yielded the second oldest exposure age, implying the bimodal distribution is not simply due to morphostratigraphic position. The reason for the bimodal distribution is thus not clear. Perhaps ice has reached more or less the same location twice. Another possibility is that the younger two boulders may have been affected by differential snow shielding, or post-depositional exhumation. However, ZAP1006, the smallest sample collected, yielded the oldest exposure age (Tables 2 and 3). Substantial differences in weathering could be responsible for the age distribution, but no obviously weathered boulders were sampled at NZG, especially in light of the magnitude of erosion needed (i.e., over the last 1000 years) to cause the age range we observe. Boulder rolling could have also affected the ages obtained but sampled boulders were in rather stable positions. ^{10}Be inheritance from previous exposure, before being incorporated by the glacier (that is, not including a prior moraine limit overrun), could also have affected the obtained ^{10}Be ages; but sampled rocks showed signs of glacier abrasion that should counteract this effect, and plus each sample may contain a unique amount, which is not apparent in the bimodal distribution. Whatever the cause, we do not calculate a mean for the ^{10}Be age population. Taken at face value, the ^{10}Be ages suggest that the NZG oscillated close to its last major Holocene maximum between ca. 670 and 330 yr. B.P., with glacial advances occurring at 600 ± 70 yr. B.P. and 340 ± 20 yr. B.P. In this scenario, the ice advanced to the TDP VII outer ice maximum position at two different times. It is possible that the later of these advances at 340 ± 20 yr. B.P. could have overridden part of the moraine that contains ZAP1007 (590 ± 40), without significant reworking (cf., Piotrowski et al., 2004). In this case, the overall age distribution supports the TDP VII moraine being a composite landform built during more than one glacial advance recorded.

5.3. Holocene glacier fluctuations in Torres del Paine

The probability distribution of our ^{14}C data, along with the morphostratigraphic context, allow us to define three distinct ages for glacial expansions in Torres del Paine as defined by the peak calibrated ^{14}C ages at 3210 yr, 720 yr, and 190 yr. B.P. (Fig. 8). We therefore assume that Tyndall, Pingo, and Zapata Glaciers advanced at these times. Where we have both ^{14}C and ^{10}Be ages for the same moraines (i.e., NZG), the two datasets agree closely. For instance, the close-maximum ^{14}C ages obtained from the inner TDP VII moraines (4 samples: ZAP0902, ZAP0903, ZAP0904, ZAP0905) are consistent with the ^{10}Be ages, with both indicating an advance as early as 700 yr. B.P. (Fig. 5B). We did not find any evidence for a glacial advance at ca. 1220 ± 160 yr. B.P. as reported by Aniya and Sato (1995a) for Zapata Glacier. Their interpretation was based on a ^{14}C age from a dead standing tree along Río Doña Rosa close to our sampled *in situ* trees (samples ZAP1401A, ZAP1402, ZAP1405, ZAP1407A; Table 1, Fig. 1), which all produced younger ages. However, the exact location was not specified, and thus we cannot make a direct comparison between their data and ours. Glacier

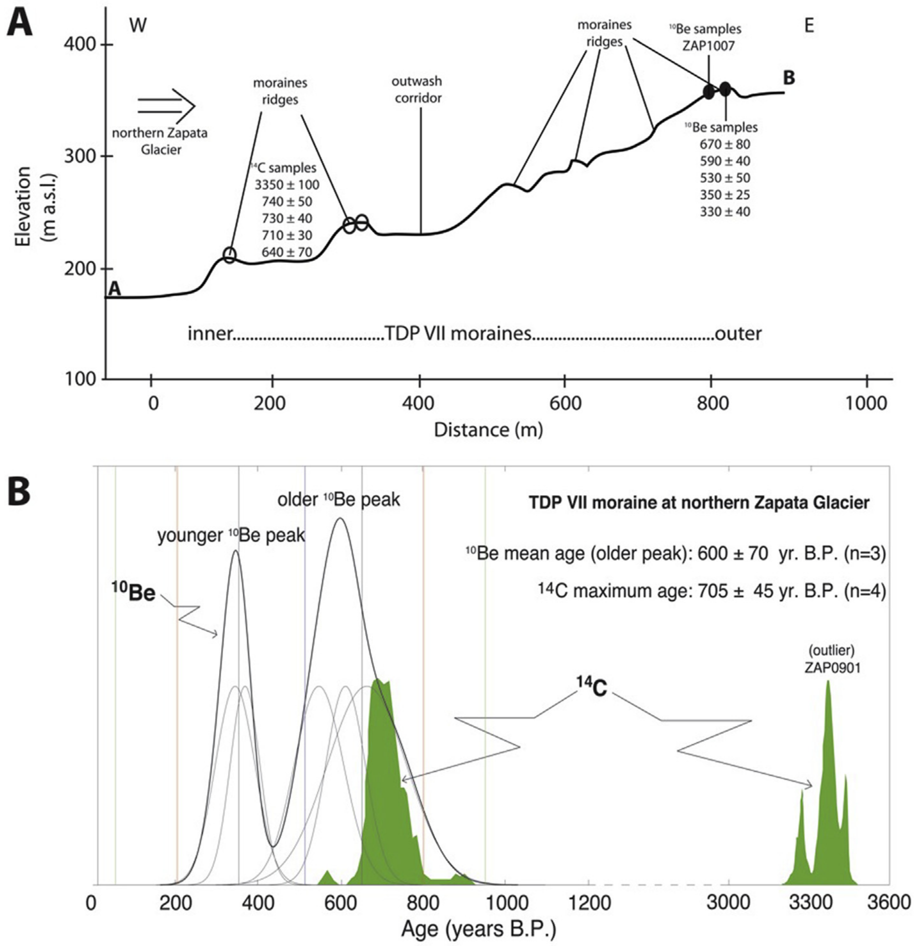

Fig. 5. Composite ^{14}C and ^{10}Be dating of the TDP VII moraine belt at northern Zapata Glacier. A Topographic profile across the TDP VII moraine including the location of ^{14}C samples (empty circles) and ^{10}Be samples (closed circles). See profile location in Fig. 1D (white dashed line). **B** Probability density plot displaying individual ^{10}Be (thin inner lines; ages referenced to 1950) and associated peak ^{10}Be ages plotted against the summed ^{14}C calibrated maximum age (solid green curve) obtained for the TDP VII moraine belt at northern Zapata Glacier (samples ZAP0902-to-0905). Collectively, the ^{14}C and ^{10}Be ages afford evidence for both a maximum limiting and direct age control, respectively, for this landform. One of these wood samples (ZAP0901) was obtained from the innermost TDP VII ridge and yielded and age >2500 years older than the other ^{14}C maximum and the ^{10}Be ages of the TDP VII moraine and therefore it is not included in our discussion. (For interpretation of the references to colour in this figure legend, the reader is referred to the Web version of this article.)

advances at ca. 1100−1400 yr. B.P. have been reported in other Patagonian glaciers including SPIF outlet glaciers nearby at Lago Argentino and Cordillera Darwin (e.g., Strelin et al., 2014; Kaplan et al., 2016; Aniya, 1995; Hall et al., 2019), suggesting that SPIF outlet glaciers in Torres del Paine probably also did advance at about this time. Nonetheless, more data are required to confirm this SPIF expansion in Torres del Paine. Therefore, the combined ^{14}C −^{10}Be Zapata Glacier record, together with those we obtained around Pingo and Tyndall Glaciers, suggests advances at ≤3210 yr. B.P., 1220 ± 160 yr. B.P. (Aniya and Sato, 1995a), 600 ± 70 yr. B.P., 340 ± 20 yr. B.P. and ≤190 yr. B.P. in Torres del Paine. Each of these advances interrupted warmer periods between ca. 3500−3100 yr. B.P., ca. 900 - 650 yr. B.P. and between ca. 350 and 200 yr. B.P., as indicated by ^{14}C-dated forest wood (Table 1) bulldozed into glacial deposits.

Although we cannot link all the ^{14}C-dates to distinct TDP landforms, our chronology helps to constrain the timing and extent of readvances that ended with the deposition of the TDP VI and TDP VII moraines. ^{10}Be dating of the TDP VII moraines at Zapata Glacier provides direct chronologic evidence for the earliest age of this moraine belt at 600 ± 70 yr. B.P. (Fig. 5B). In addition, indirect radiocarbon dating of this landform provides evidence that the innermost TDP VII ridges at Pingo and Tyndall Glaciers were deposited at ≤190 yr. B.P., constraining the age of the whole TDP VII moraine complex at the three glaciers (Zapata, Pingo and Tyndall) to between 600 ± 70 yr. B.P. and ≤190 yr. B.P. In other words, each of these ice advances contributed to the formation of the TDP VII moraine complex. The outer TDP VI moraine still lacks direct dating. Based on available ^{14}C-dated stratigraphic evidence, it is possible that this landform was built by the advances at ≤3210 yr. B.P. and/or at ca. 1200 yr. B.P. as recorded by Zapata Glacier.

Our Holocene glacial chronology, together with those from earlier studies in the area, reveals a more comprehensive history than previously appreciated for Torres del Paine glaciers. Both Pingo and Zapata Glaciers likely merged with Grey Glacier to build the TDP V moraine enclosing Lago Margarita, about 15 km down valley from TDP VI moraines of the Pingo Glacier (Marden and Clapperton, 1995; García et al., 2014). The age of the TDP V moraine remains poorly constrained, but minimum ^{14}C ages suggest that several glacial advances built this moraine system during the Early to Mid Holocene, between >9740 ± 190 and >3810 ± 85 cal. yr. B.P. (Moreno et al., 2009; Marden and Clapperton, 1995). Glacier retreat from the TDP V moraines occurred before 3810 ± 85 yr. B.P., as inferred a basal age from a mire located inboard from these

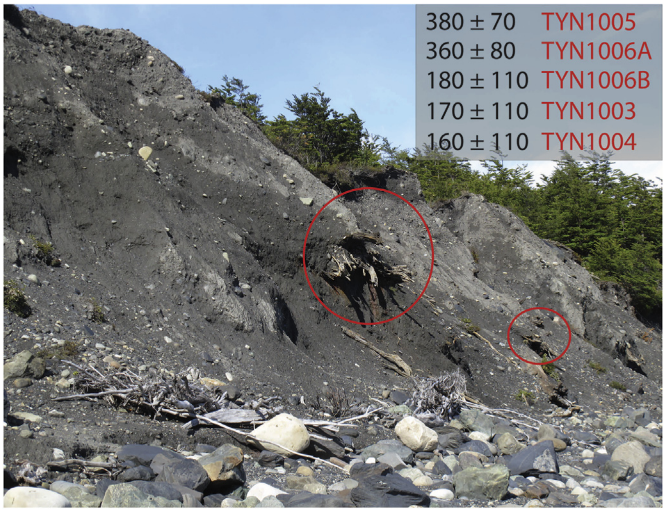

Fig. 6. Radiocarbon dates on the innermost ice-contact slope fronting Lago Geike, Tyndall Glacier. The picture displays groups of ripped up wood fragments and twigs and their calibrated ^{14}C age (2 sigma error). This section is within the TDP VII moraine representing the last prominent readvance of Tyndall Glacier.

landforms near Grey Glacier (Moreno et al., 2009). This age is identical to another basal minimum limiting age of 3890 ± 260 yr. B.P. obtained by Aniya and Sato (1995a) in a mire distal to the TDP VII ice margin at Zapata Glacier (Fig. 1). Both ages represent local ice-free conditions and suggest that ice retreated before this time in response to climate amelioration. After at least 600 years of forest development, the Torres del Paine Glaciers readvanced at ≤3210 yr. B.P. and then at 1220 ± 160 yr. B.P., when the TDP VI moraine may have been built.

The new chronology obtained from several sites at NZG allows us to constrain times of glacier reduction and forest colonization at ~1200–700 years B.P. (Table 1). Following this period of reduced glacier extent, the last set of major Holocene advances began, the first of which culminated at 600 ± 70 yr. B.P., as indicated by the ^{10}Be ages from NZG TDP VII moraines. Another culmination seems to have occurred at 340 ± 20 yr. B.P., based on the younger ^{10}Be ages from the TDP VII moraine at NZG. Nearby in Torres del Paine, Grey and Francés Glaciers also advanced at about this time (Röthlisberger, 1986; Marden and Clapperton, 1995). This glacier culmination was followed by ice-front oscillations that allowed local forest growth, which was subsequently overrun by historical readvances after ca. 200 yr. B.P., as recorded by Pingo and Tyndall Glaciers (Table 1). In AD 1944, the NZG front was only ~1 km inboard of the innermost TDP VII moraine ridge (Aniya and Sato, 1995a), with most ice front retreat occurring afterwards.

5.4. Middle to Late Holocene glacier fluctuations in Patagonia

Prominent Mid-Holocene advances in the region between about 7000 and 4000 yr. B.P. are recorded just to the north around the Lago Argentino and Torre Glaciers (49-50°S) (Aniya, 1995; Mercer, 1970; Strelin et al., 2014; Kaplan et al., 2016; Reynhout et al., 2019). Farther north, the Río Tranquilo Glacier (Monte San Lorenzo, 47 °S deposited the RT6 moraine by 5.7 ± 0.1 ka (Sagredo

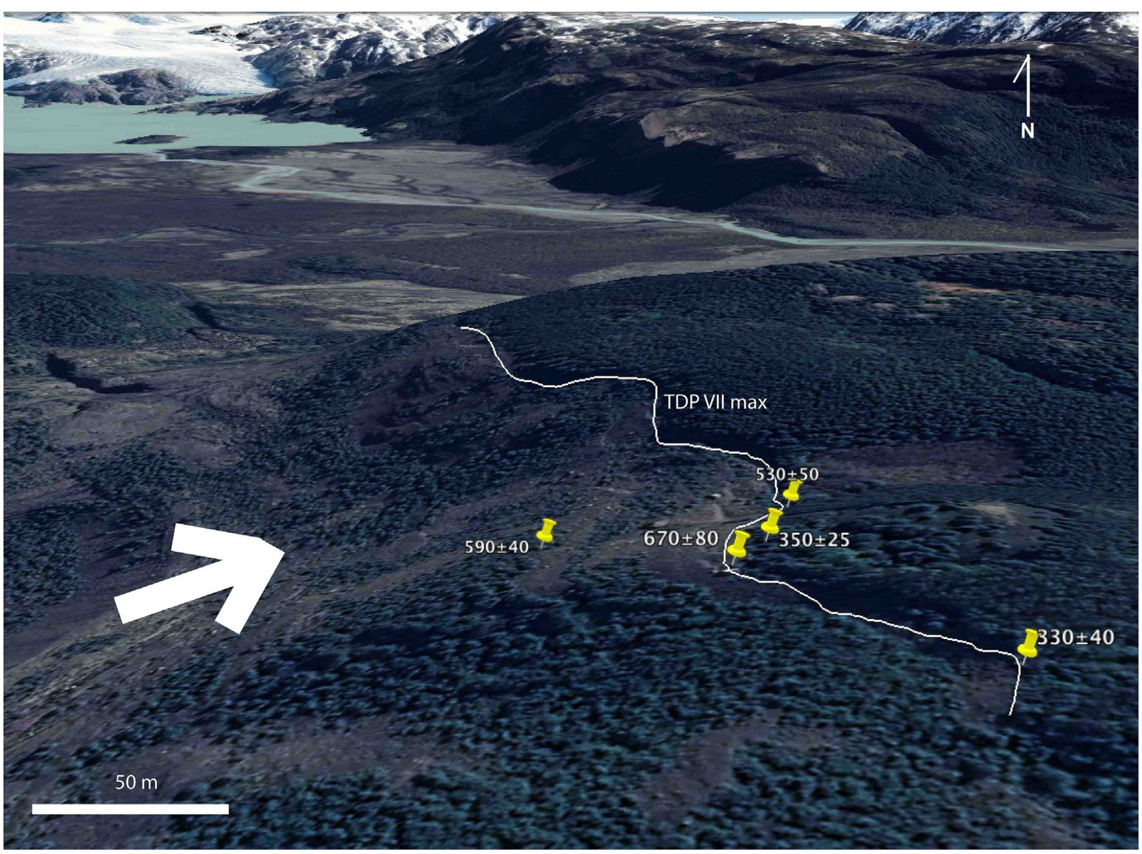

Fig. 7. Google Earth satellite image showing the distribution of the ^{10}Be samples and ages obtained for the Zapata Glacier. The white line is the mapped maximum extent of the northern Zapata Glacier (NZG) (located to the left of the Google Image, not shown), the TDP VII moraine. White arrow indicates direction of ice flow. Pingo Glacier is in the background.

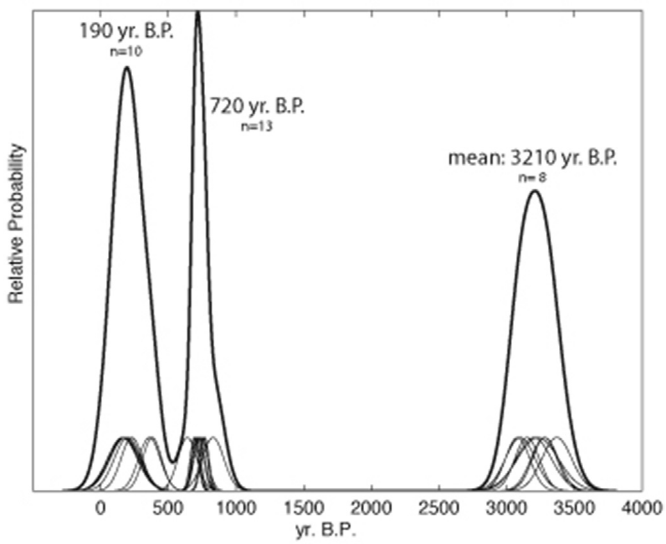

Fig. 8. Relative probability distribution of all ^{14}C maximum dates obtained from wood embedded in till, outwash sediments and in-situ tree stumps at Zapata, Tyndall and Pingo Glaciers (this study). Also shown are the associated mean ages of SPIF glacial advances as discussed in the text. Individual lines are single sample relative probabilities and thick lines are the summed probability peak age for glacial advances.

et al., 2016). Similarly, the Colonia outlet Glacier (eastern North Patagonian Ice field, 47°S) deposited the moraine enclosing the Lago Colonia by 5.4 ± 02 ka (Nimick et al., 2016). These Middle Holocene expansions are coincident with a drop in nearby SST and a peak in *Nothofagus* expansion in south Patagonia (Caniupán et al., 2014; Moreno et al., 2010, 2018). We did not find evidence of these advances in our study but infer that moraines of this age may correspond to the TDP V moraine belt enclosing Lago Margarita, beyond our study area, based on the minimum basal ^{14}C age in Moreno et al. (2009). After the Mid Holocene ice expansions, Patagonian outlet glaciers retreated close to or within present-day ice margins at about 3800 yr. B.P. (e.g., Zapata Glacier, Aniya and Sato, 1995a; Moreno and Hammick Glaciers, Mercer, 1970; 1968). This glacier retreat coincided with open woodland and expansion of grassland indicative of warm and dry climate in south Patagonia (Moreno et al., 2009, 2018). A subsequent ice advance culminated after 3200 yr. B.P., as dated by this study at NZG, and potentially linked to the formation of the TDP VI moraine. Colder and wetter conditions peaked nearby, close to Lago Grey (Fig. 1), by this time as also evidenced by the presence of closed-canopy Magellanic forest along with high lake levels (Moreno et al., 2009). The new glacier record adds significantly to previously available chronologies between about 3000–2000 yr. B.P. for this expansion in Patagonia, which deposited multiple moraines or glacial sediments on both sides of the SPIF (e.g., Strelin et al., 2014; Aniya, 1995; Clapperton and Sugden, 1988; Geyh and Röthlisberger, 1986; Mercer, 1970, 1965). It is possible that this glacial expansion culminated at several different times between ca. 3200–2000 yr. B.P., depending on the Patagonian site (cf., Hall et al., 2019; Menounos et al., 2020). Retreat after 2000 yr. B.P. seems to have been widespread (Mercer, 1968), allowing peat accumulation and *Nothofagus* growth on recently deglaciated terrain. Prior to the last millennium, dated Holocene ice advances occurred ~1500 to ~1100 yr. B.P. and were widespread in the southern Patagonian Andes, including Cordillera Darwin (Kaplan et al., 2016; Strelin et al., 2008, 2014; Hall et al., 2019; Aniya and Sato, 1995a; Röthlisberger, 1986; Mercer, 1965).

5.5. Glacier fluctuations during the last millennium in Patagonia

Tree rings, pollen, lichens, and glaciers have documented climate changes during the last 1000 years in Patagonia. The terrestrial and marine record for this period is well preserved and provides a unique opportunity for detailed research on the climate-ocean-ice linkages (e.g., Kilian and Lamy, 2012). Our record builds on these archives and altogether reveals three distinct centennial-scale climate oscillations that punctuated the last millennium (LM): the *early, middle* and *final* glacial stages (Fig. 9). Abundant ^{14}C ages of wood from about 1000 to 650 yr. B.P. represent an ice-free period consistent with warmer and drier conditions. This is supported by pollen (reduced *Nothofagus* forest) and lake sediment proxies in the Torres del Paine and from *Fitzroya cupressoides* tree rings in north Patagonia (Villalba, 1994, Moy et al., 2008; Moreno et al., 2014). Climate deterioration followed and favored Patagonian glacier expansion between ca.750-500 yr. B.P. during the *early* LM stage (Fig. 9). At this time, pollen and tree ring records show enhanced humid and cool conditions (e.g., cold summers), when Patagonian glaciers between at least 41–54 °S expanded (Mercer, 1970; Röthlisberger, 1986; Villalba, 1990, 1994; Aniya and Sato, 1995b; Glasser et al., 2002; Strelin et al., 2014; Kaplan et al., 2016; Reynhout et al., 2019; Hall et al., 2019). After a short warm period with general glacial recession, another centennial-scale cold phase led to widespread Patagonian glacier expansion that culminated ca. 400-300 yr. B.P. during the *middle* LM stage (this study; Villalba, 1994; Luckman and Villalba, 2001; Masiokas et al., 2009). At Lago Argentino, to the north, an event is ^{10}Be dated to 300 ± 30 years (Kaplan et al., 2016, relative to 1950), statistically similar to Torres del Paine where we suggest an age of 340 ± 20 years. Again, glaciers in the northern and southern Patagonian Andes between 41 and 54 °S expanded at about this time (Fig. 9). Glacier retreat followed (Figs. 5 and 8), which was again reversed by renewed glacier expansion after 250-200 yr. B.P. in the *final* LM stage; this is the last cold phase recorded at Torres del Paine and around the southernmost sector of the SPIF, as well as elsewhere in Patagonia (Fig. 9) (Mercer, 1982; Villalba, 1994; Villalba et al., 2005; Masiokas et al., 2009; Caniupán et al., 2014; Kaplan et al., 2016; Meier et al., 2018; Menounos et al., 2020).

An important unanswered question has been when Patagonian glaciers reached their Late Holocene maximum extent during the last millennium. It is commonly assumed that glaciers reached their maximum Late Holocene last millennium expansion between the 16–19th Centuries. However, as described above, tree rings and pollen paleoclimate proxies suggest a peak of cold temperatures (as much as 2 °C lower than present) and humid conditions much earlier at ~650 yr B.P. *Nothofagus*-dominated forest reached a maximum at this time in response to concurrent cold and humid conditions, and gradually retreated afterwards (Moreno et al., 2014). Most of the available glacier constraints are based on ^{14}C dated wood in stratigraphic contexts and tree rings, and direct dating of Patagonian Holocene moraines is sparse. However, our study, which relies on direct dating of moraines and till by close-maximum ^{14}C ages and ^{10}Be on boulders, uncovers a glacial maximum during the last millennium as early as 600 ± 70 yr. B.P. (Fig. 9). A maximum latest Holocene glacial extent at this time also has been found in the nearby Lago Argentino Basin (50°S). Here, boulders resting on the outer Pearson 2a (Península Herminita) and Frías 2a moraine crests range between 650 and 500 yr. B.P., and date the greatest extent of the Upsala and Frías Glaciers (Strelin et al., 2014; Kaplan et al., 2016). This evidence suggests that south Patagonian glaciers not only advanced by this time, but they also reached their maximum over the last millennium at this time. Whether or not the northern Patagonian glaciers advanced in

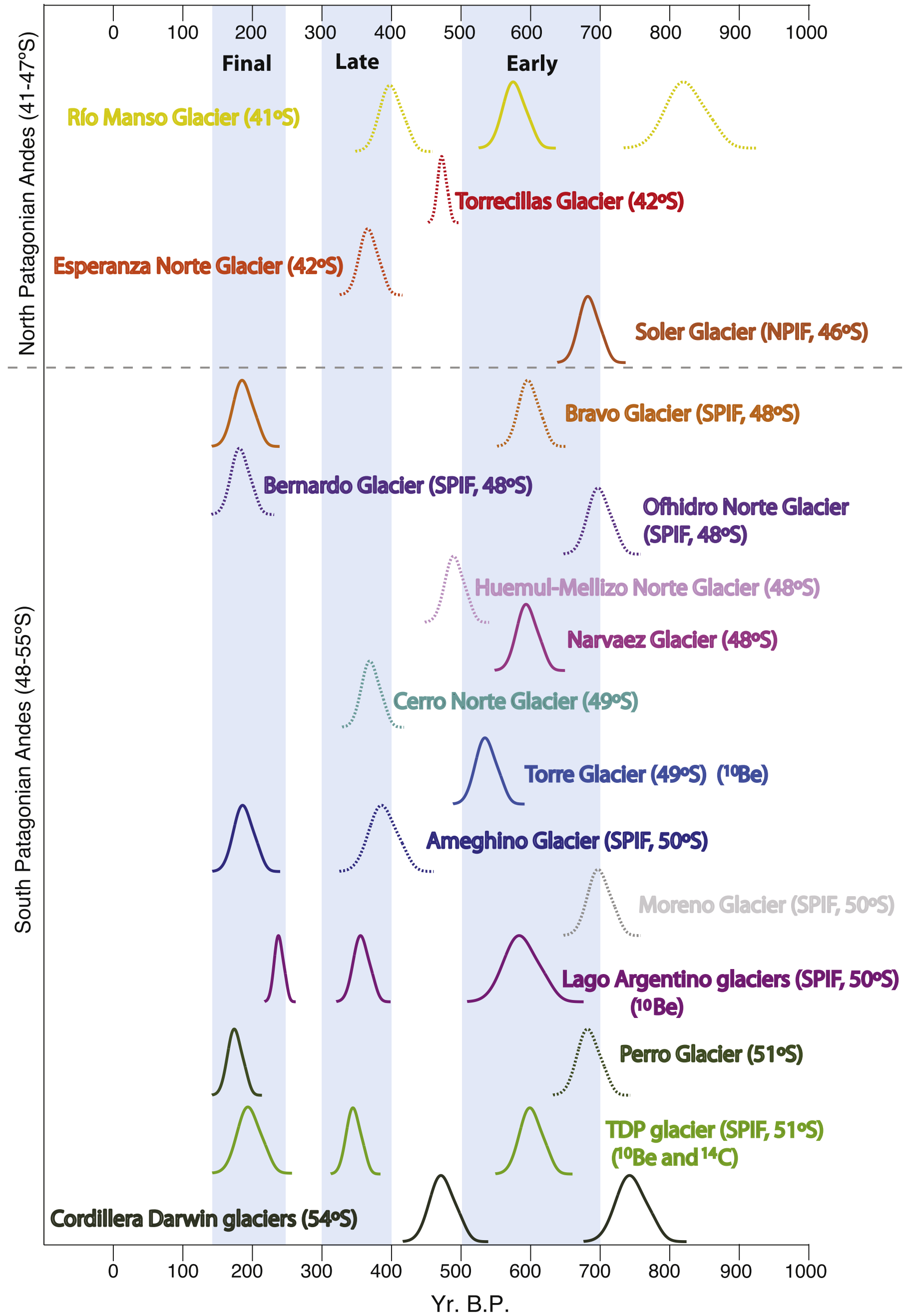

Fig. 9. Glacier advances in the Patagonian Andes during the last millennium. All records shown in the figure, except for TDP (Zapata, Tyndall, Pingo), Lago Argentino and Torre glaciers, obtained exclusively from ^{14}C dated *in situ* stumps overridden during a glacier advance. These records represent close-maximum ages for the respective glacier expansion interpreted to have killed the trees. Cordillera Darwin record is based on close maximum ^{14}C ages of wood in till (Hall et al., 2019). Plotted probability distributions include the ^{14}C calibrated 1 sigma age range. When more than one probability range was produced with the ^{14}C age calibration, we plotted the one with higher probability; solid probability distribution lines indicate the mean of two or more ^{14}C ages, whereas dotted lines indicate a single ^{14}C age. For the TDP (i.e., Zapata Glacier, this study), Lago Argentino (Kaplan et al., 2016) and Torre glaciers (Reynhout et al., 2019) the summed probability distributions obtained from multiple ^{10}Be ages are shown. The younger advance of TDP glaciers (Pingo and Tyndall) is based on multiple ^{14}C close-maximum data (Table 1). Perro, Huemul-Mellizo Norte, Bravo, Río Manso Glaciers (Röthlisberger, 1986); Ameghino, Narvaez, Esperanza Norte and Torrecillas Glaciers (Masiokas et al., 2000, 2001 and 2009); Moreno glacier (Aniya and Sato, 1995b); Bernardo, Cerro Norte and Ofhidro Norte Glaciers (Mercer, 1965, 1970); Soler Glacier (Glasser et al., 2002). Outlet glaciers draining the NPIF (North Patagonian Ice field) or the SPIF (South Patagonian Ice Field) are indicated. The limit between the North Patagonian and South Patagonian Andes at 48°S is based on the geographic occurrence of present-day ice fields. Blue vertical bars indicate Patagonian glacier advance periods during the *early*, *late* and *final* last millennium glacial stages. (For interpretation of the references to colour in this figure legend, the reader is referred to the Web version of this article.)

synchrony cannot be confirmed with the available data, but it cannot be ruled out (cf., Masiokas et al., 2009). Moreover, glaciers could have occupied the same maximum ice-marginal positions at different times during the last millennium implying that similar climate conditions occurred several times within this period (Hall et al., 2019). For instance, our data suggest that the Zapata Glacier readvanced to build the TDP VII moraine at ca. 340 yr. B.P. to reoccupy the prior maximum extent reached before at ca. 600 yr. B.P.

5.6. European Little Ice Age

The latest Holocene includes a period when world-wide glaciers readvanced and deposited moraines. In the northern hemisphere this period is designated as the Little Ice Age (LIA), but many times this term is used to designate similar-age moraines elsewhere in the southern hemisphere, including in Patagonia. The LIA glacier chronologies from the European Alps indicate major glacier expansions by the middle XVII and XIX centuries (e.g., Zumbuhl and Nussbaumer, 2018), thus similar to glaciers in Patagonia and New Zealand (Schaefer et al., 2009). Nonetheless, the northern hemisphere pattern of Holocene glaciation differs from that in the south. Whereas in the north a long-term Holocene cooling occurs, with the LIA moraine being the most extensive Middle to Late Holocene glacier advance, in the south, at least from Middle Holocene to present, a net warming trend is recorded, with the last millennium moraine advances being the least extensive. Interhemispheric asynchronic glaciers are apparent within the Late Holocene glacial records (Putnam et al., 2012; Kaplan et al., 2016). Whereas the pattern of Holocene glaciation in the European Alps has been recognized elsewhere in the northern hemisphere (Wiles et al., 2008), differences within the southern hemisphere may occur. The latter is suggestive of regional forcing and/or amplifying climate mechanisms (Schaefer et al., 2009). Altogether, available evidence shows that despite a distinct interhemispheric climate cooling recorded by moraines occurred during past centuries (i.e., between about 1300–1850 AD), differences between glacier records exist that at present precludes a comprehensive understanding of underlying drivers of climate change, including the Late Holocene European LIA (cf., Hall et al., 2019). In the light of this work in progress, we recommend the clarifying term “European Little Ice Age”, or “Little Ice Age chronozone” when comparing northern records with the southern hemisphere Late Holocene moraine record.

5.7. Forcing mechanisms and Antarctic connections

The SWW and associated storm circulation system exert a main control on Patagonian temperature and precipitation and therefore on glacier dynamics. General Patagonian net glacier retreat since the mid-20th century coincides with overall lower precipitation rates and warmer air temperatures (Garreaud et al., 2013; Carrasco et al., 2002). In the most recent decades, this climate signal has been associated with a positive phase of the SAM, which is the main mode of climate variability at this latitude affecting the low-level tropospheric SWW strength. The SAM represents a mode of oscillation that compares the atmospheric sea level pressure at Antarctic and mid-latitude locations, and therefore helps explain low-level tropospheric variability south of about 20°S (i.e., the extratropics). The positive phase of the SAM occurs when a lower than the mean pressure is found in Antarctica and a higher than the mean value occurs in the mid-latitudes. This phase is characterized by summer strengthened SWW zonal circulation in southernmost South America and the Southern Ocean bringing higher than average air temperatures and precipitation south of ~50°S (e.g., Garreaud et al., 2013). Under the same SAM positive phase, the Patagonian region between about 40 and 50 °S is characterized by summer diminished SWW strength, higher air temperatures and lower precipitation on the Pacific side. The reverse climate conditions occur during the SAM negative phase (Garreaud, 2007).

Some studies attributed SAM’s recent positive trend to ozone depletion (Thompson and Solomon, 2002; Thompson et al., 2011; Previdi and Polvani, 2014) although the regional trend in winds can be also partially attributed to tropical SST changes through the Rossby wave mechanism at multidecadal time scales (Yuan et al., 2018). Different lines of paleoclimate evidence show that the Holocene has been characterized by distinct centennial-scale dry/warm and wet/cold cycles that mimics a SAM type of variability (e.g., Moreno et al., 2014, 2018). This implies that the SWW fluctuated in association with these climate patterns to drive Patagonian climate and glacier fluctuations (Reynhout et al., 2019). As described above, the last ~1000 years until ~150 yr. B.P. were characterized by distinct dry/warm (i.e., south shifted SWW) and wet/cold (north shifted) cycles, recorded by Torres del Paine glaciers.

On the Antarctic Peninsula, warm/cold climate oscillations have also been recorded by glacier fluctuations, as well as by proxies, such as lake sediments, sea-ice coverage, moss banks, pollen, and marine and ice-core records (e.g., Kreutz et al., 1997; Bentley et al., 2009; Hall, 2009; Hall et al., 2010; Pike et al., 2013; Kaplan et al., 2020; Shevenell and Kennett, 2002). We now compare these with the Patagonian glacier record in order to assess the latitudinal phasing of climate change and its possible cause. Between about 4500–3000 yr. B.P. a general interval of warmth associated with reduced glaciers at times (and local ice shelves absent in Antarctica) followed a glacier expansion in both Patagonia and Antarctic Peninsula (e.g., Hall, 2009; Bentley et al., 2009; Davies et al., 2014; Reynhout et al., 2019; Kaplan et al., 2020). After about 3000 yr. B.P. Patagonian and Antarctic glaciers readvanced associated with cooling (e.g., this study, Domack and McClennen, 1996; Domack et al., 2001; Hall, 2009; Kaplan et al., 2020). Direct moraine dating using terrestrial cosmogenic nuclides indicates a subsequent glacier expansion on King George Island and James Ross Island between ~1500 and 1100 yr. B.P., consistent with the Patagonian glacier history (Hall, 2009; Davies et al., 2014; Hall et al., 2019; Kaplan et al., 2020). Between about 1100 and 700 yr. B.P. glaciers in the Antarctic Peninsula were again reduced in extent (e.g., Bentley et al., 2009; Hall et al., 2010) and then exhibited a major readvance, at and after 650 yr B.P. as in Patagonia (e.g., this study; Clapperton and Sudgen, 1988; Hall, 2007; Kaplan et al., 2020). Glacier retreat has occurred through the last decades in Patagonia and Antarctic Peninsula, with both areas affected by warming air and ocean temperatures (Garreaud, 2007; Marshall et al., 2006; Gille, 2008; Davies et al., 2014; Turton et al., 2018).

We hypothesize that changes in the position/strength of the SWW at the sub-millennial timescale forced broadly concurrent Holocene glacier and climate fluctuations in Patagonia and in the Antarctic Peninsula, as it does at present (Fyfe et al., 2007; Marshall and Speer, 2012; Rignot et al., 2019). Strengthened sub polar SWW pushes the warm upper circumpolar deep water (CDW) towards the Antarctic Peninsula, where it is transported from the slope through submarine canyons to the shelf where marine terminating glaciers occur (Martinson et al., 2008; Rignot et al., 2019). Warmer and shallower CDW on the continental shelf of West Antarctica result in enhanced basal ice-shelf melt (thus reducing glacier buttressing), thinning and grounded glacier acceleration (Pritchard et al., 2012; Rignot et al., 2019). This mechanism makes glacier response along west Antarctic Peninsula sensitive to SST change, likely forced by SWW fluctuations (Fyfe et al., 2007; Marshall and Speer, 2012; Cook et al., 2016; Rignot et al., 2019). Enhanced upwelling of CDW reduces sea ice extent/thickness allowing an amplified ocean-atmosphere heat exchange, warming in Antarctic Peninsula, and glacier breakdown (Toggweiler et al., 2006; Fyfe et al., 2007; Martinson et al., 2008; Marshall and Speer, 2012). Also, intensified poleward shifted SWW is associated with glacier meltdown in eastern Antarctic Peninsula through the direct effect of foehn winds in surface melting of glaciers (e.g., Marshall et al., 2006; Turton et al., 2018).

Therefore, it seems feasible that Holocene glacier expansions sensitively responded each time that AP and Patagonia climate were affected by the SWW when they are in a cold-phase dynamic or position (e.g., SAM negative phase-like conditions). In Patagonia, an extended SWW is linked to a northward shifted and/or slower ACC, expanded sea ice, and increased advection of Sub-Antarctic cold water northward along the Pacific coast of southern South America through the Humboldt Current (cf., Domack et al., 2001; Lamy et al., 2002, 2015). Moreover, during these cold periods, the northward- extended SWW also caused advection of cold water into the Patagonian fjords (Caniupán et al., 2014) with the expected positive effects on the ice field's mass balance and extent.

6. Conclusions

Our combined $^{14}C-^{10}Be$ study on the southern margin of the South Patagonian Ice Field at Torres del Paine National Park allows the following conclusions:

- The glacier record at Torres del Paine suggests that the SPIF expanded at $\leq$3210 yr. B.P., 600 $\pm$ 70 yr. B.P., 340 $\pm$ 20 yr. B.P. and $\leq$190 yr. B.P. Glacial advances interrupted warm periods when forest was growing along the ice margin between ca. 3500–3100 yr. B.P., ca. 900 - 650 yr. B.P., and between ca. 350 and 200 yr. B.P.
- The last set of major Late Holocene advances was underway by ca. 600 yr. B.P, based on 14 new maximum limiting ^{14}C and three ^{10}Be ages; this was the maximum of the last millennium glacial advances, although ice reached close to the same position again at ca. 340 yr. B.P.
- Multi-proxy paleoclimate evidence points to a Late Holocene period punctuated by marked centennial scale warm/dry and cold/wet climate fluctuations, with main Patagonian glacial expansions by 700–500 yr. B.P., 400–300 yr. B.P. and 250-150 yr. B.P. during the *early, late* and *final* last millennium glacial stages.
- We infer that broadly in-phase Holocene variation of the Patagonian and Antarctic Peninsula glaciers followed the change in the strength of the SWW through the position and oceanographic conditions of the ACC in the Southeast Pacific. Glacier advances in both regions are consistent with a north shifted SWW. For Patagonia, such climate mode increased advection of ACC cold water northward along the SE Pacific coast associated with cooler and wetter atmospheric conditions. For the Antarctic Peninsula, northward shifted SWW inhibited the upwelling of warmer Circumpolar Deep Water in the Southern Ocean, favouring surface ocean cooling and sea ice expansion.

Authors credit

JLG conceived the project. JLG, GAG and VJG collected the ^{10}Be and ^{14}C samples. JLG, MRK, BLH, RS and JMS performed the ^{10}Be laboratory work. JLG, BLH, and RDP-H performed the ^{14}C laboratory work. JLG, MRK, BLH interpreted the data. All authors contributed to writing the paper.

Declaration of competing interest

The authors declare that they have no known competing financial interests or personal relationships that could have appeared to influence the work reported in this paper.

Acknowledgements

This research received funding by the GSA Quaternary Geology & Geomorphology Division and FONDECYT Grant 1161110 (JLG) and NSF EAR 09–02363 (MRK and JMS). We thank Tomás Rojo and Carmen Daggett for assistance in the field. We also thank the Corporación Nacional Forestal (CONAF) of Chile and the Administration of the Torres del Paine National Park for supporting this research. We appreciate and thank the comments by reviewers Dr. Bethan Davies and Dr. Harold Lovell that helped to improve the quality of this paper. This is LDEO Contribution 8438.

References

Aniya, M., 2013a. Holocene glaciations of hielo patagónico (patagonian icefield), south America: a brief review. Geochem. J. 47, 97–105.
Aniya, M., 1995. Holocene glacial chronology in Patagonia: Tyndall and Upsala glaciers. Arct. Alp. Res. 27, 311–322.
Aniya, M., 2013b. Holocene glaciations of hielo patagónico (Patagonia icefield), south America. A brief review. Geochem. J. 47, 97–105.
Aniya, M., Sato, H., 1995a. Holocene glacier variations at Tyndall Glacier area, southern Patagonia. Bulletin of glacier research 13 97–109.
Aniya, M., Sato, H., 1995b. Holocene glacial chronology of Upsala glacier at Peninsula Herminita, southern Patagonia. Bull. Glaciol. Res. 13, 83–96.
Balco, G., Stone, J.O., Lifton, N.A., Dunai, T.J., 2008. A complete and easily accessible means of calculating surface exposure ages or erosion rates from ^{10}Be and ^{26}Al measurements. Quat. Geochronol. 3, 174–195.
Barcaza, G., Nussbaumer, S., Valdés, J., Tapia, G., García, J.L., Videla, Y., Albornoz, A., Arias, V., 2017. Glacier inventory and recent glacier variations in the Andes of Chile, South America. Ann. Glaciol. 58, 166–180.
Bentley, M., Hodgson, D., Smith, J.A., Cofaigh, C.O., Domack, E., Larter, R.D., Roberts, S.J., Brachfeld, S., Leventer, A., Hjort, C., Hillenbrand, C.D., Evans, J., 2009. Mechanisms of Holocene palaeoenvironmental change in the Antarctic Peninsula region. Holocene 19, 51–69.
Caniupán, M., Lamy, F., Lange, C., Kaiser, J., Kilian, R., Arz, H.W., León, T., Mollenhauer, G., Sandoval, S., De Pol-Holz, R., Pantoja, S., Wellner, J., Tiedemann, R., 2014. Holocene sea-surface temperature variability in the Chilean fjord region. Quat. Res. 82, 342–353.
Carrasco, J., Casassa, G., Rivera, A., 2002. Meteorological and climatological aspects of the southern Patagonia ice Cap. In: Casassa, G., Sepúlveda, F.V., Sinclair, R.M. (Eds.), The Patagonian Icefields: A Unique Natural Laboratory for Environmental and Climate Change Studies. Kluwer Academic, pp. 29–41.
Clapperton, C.M., Sugden, D.E., 1988. Holocene glacier fluctuations in South America and Antarctica. Quat. Sci. Rev. 7, 185–198.
Cook, A.J., Holland, P.R., Meredith, M.P., Murray, T., Luckman, A., Vaughan, D.G., 2016. Ocean forcing of glacier retreat in the western Antarctic Peninsula. Science 353, 283–286.
Davies, B.J., Golledge, N.R., Glasser, N.F., Carrivick, J.L., Ligtenberg, S.R.M., Barrand, N.E., van den Broeke, M.R., Hambrey, M.J., Smellie, J.L., 2014. Modelled glacier response to centennial temperature and precipitation trends on the Antarctic Peninsula. Nat. Clim. Change 4, 993–998.
Davies, Bethan J., Darvill, Christopher M., Lovell, Harold, Bendle, Jacob M., Dowdeswell, Julian A., 2020. The evolution of the Patagonian Ice Sheet from 35 ka to the present day (PATICE). Earth Sci. Rev. 204, 103152.
Domack, E.W., McClennen, C.E., 1996. Accumulation of glacial marine sediments in fjords of the Antarctic Peninsula and their use as late Holocene paleoenvironmental indicators. In: Ross, R., Hoffman, E., Quetin, L. (Eds.), Foundations for Ecosystem Research West of the Antarctic Peninsula. American Geophysical Union, Washington DC, pp. 135–154.
Domack, E., Leventer, A., Dunbar, R., Taylor, F., Brachfeld, S., Sjunneskog, C., 2001. Chronology of the palmer deep site, Antarctic Peninsula: a Holocene palaeoenvironmental reference for the circum-Antarctic. Holocene 11, 1–9.
Eyles, N., Eyles, C.H., Miall, A.D., 1983. Lithofacies types and vertical profile models; an alternative approach to the description and environmental interpretation of glacial diamict and diamictite sequences. Sedimentology 30, 393–410.
Evans, D.J.A., Phillips, E.R., Hiemstra, J.F., Auton, C.A., 2006. Subglacial till: formation, sedimentary characteristics and classification. Earth Sci. Rev. 78 (1–2), 115–176.
Fyfe, J.C., Saenko, O.A., Zickfeld, K., Eby, M., Weaver, A.J., 2007. The role of poleward-intensifying winds on Southern Ocean warming. J. Clim. 20, 5391–5400.
García, J.L., Kaplan, M.R., Hall, B.H., Schaefer, J.M., Vega, R.V., Schwartz, R., Finkel, R., 2012. Glacial expansion in southern Patagonia throughout the Antarctic cold reversal. Geology 40, 859–862.

García, J.L., Brenda, L. Hall, Kaplan, Michael R., Vega, Rodrigo M., Strelin, Jorge A., 2014. Glacial geomorphology of the Torres del Paine region (southern Patagonia): implications for glaciation, deglaciation and paleolake history. Geomorphology 204, 599–616.
Garreaud, R.D., 2007. Precipitation and circulation covariability in the extratropics. J. Clim. 20, 4789–4797.
Garreaud, R., Lopez, P., Minvielle, M., Rojas, M., 2013. Large-scale control on the patagonian climate. J. Clim. 26, 215–230.
Geyh, M., Röthlisberger, F., 1986. Gletscherschwankungen der letzen 10,000 Jahre. Ein Vergleich zwischen Nord– und Sudhemisphere (Alpen Himalaya, Alaska, Südamerika, Neuseeland) (Aarau, Switzerland).
Gille, S., 2008. Decadal-scale temperature trends in the Southern Hemisphere ocean. J. Clim. 21, 2749–2765.
Glasser, N.F., Hambrey, M.J., Aniya, M., 2002. An advance of Soler Glacier, North Patagonian icefield at c. AD 1222–1342. Holocene 12, 113–120.
Glasser, N.F., Jansson, K.N., Harrison, S., Rivera, A., 2005. Geomorphological evidence for variations of the north patagonian icefield during the Holocene. Geomorphology 71, 263–277.
Hall, B.L., 2007. Late-holocene advance of the Collins ice Cap, king George Island, south Shetland islands. Holocene 17, 1253–1258.
Hall, B.L., 2009. Holocene glacial history of Antarctica and the sub-Antarctic islands. Quat. Sci. Rev. 28, 2213–2230.
Hall, B.L., Koffman, T., Denton, G.H., 2010. Reduced ice extent on the western Antarctic Peninsula at 700-970 cal. yr B. P. Geology 38, 635–638.
Hall, B.L., Lowell, T.V., Bromley, G.R.M., Denton, G.H., Putnam, A.E., 2019. Holocene glacier fluctuations on the northern flank of Cordillera Darwin, southernmost South America. Quat. Sci. Rev. 222, 10590438.
Hogg, A.G., Quan, Hua, Blackwell, Paul G., Buck, Caitlin E., Thomas P, Guilderson, Heaton, Timothy J., Niu, Mu, Palmer, Jonathan G., Reimer, Paula J., Reimer, Ron W., Turney, Christian S.M., Zimmerman, Susan R.H., 2013. Radiocarbon 55 (4), 1889–1903. https://doi.org/10.2458/azu_js_rc.55.16783.
Kaplan, M.R., Strelin, J.A., Schaefer, J.M., Denton, G.H., Finkel, R.C., Schwartz, R., Putnam, A.E., Vandergoes, M.J., Goehring, B.M., Travis, S.G., 2011. In-situ cosmogenic 10Be production rate at Lago Argentino, Patagonia: implications for late-glacial climate chronology. Earth Planet Sci. Lett. 309, 21–32. https://doi.org/10.1016/j.epsl.2011.06.018.
Kaplan, M.R., Schaefer, J.M., Strelin, J.A., Denton, G.H., Anderson, R.F., Vandergoes, M.J., Finkel, R.C., Schwartz, R., Travis, S.G., Garcia, J.L., Martini, M., Nielsen, S., 2016. Patagonian and southern South Atlantic view of Holocene limate. Quat. Sci. Rev. 141, 112–125.
Kaplan, M.R., Strelin, J.A., Schaefer, J.M., Peltiera, C., Martinic, M.A., Flores, E., Winckler, G., Schwartz, R., 2020. Holocene glacier behavior around the northern Antarctic Peninsula and possible causes. Earth Planet Sci. Lett. 534, 116077.
Kerr, A., Sugden, D., 1994. The sensitivity of the south chilean snowline to climatic change. Climatic Change 28, 255–272.
Kilian, R., Lamy, F., 2012. A review of Glacial and Holocene paleoclimate records from southernmost Patagonia (49-55_S). Quat. Sci. Rev. 53, 1–23.
Kreutz, K.J., Mayewski, P.A., Meeker, L.D., Twickler, M.S., Whitlow, S.I., Pitalwala, I.I., 1997. Bipolar changes in atmospheric circulation during the Little ice age. Science 277, 1294–1296.
Lal, D., 1991. Cosmic-ray labeling of erosion surfaces in-situ nuclide production rates and erosion models. Earth Planet Sci. Lett. 104, 424–439.
Lamy, F., Rühlemann, C., Dierk Hebbeln, D., Wefer, G., 2002. High and low latitude climate control on the position of the southern Peru-Chile Current during the Holocene. Paleoceanography 17 (2). https://doi.org/10.1029/2001PA000727.
Lamy, F., Kaiser, J., Ninnemann, U., Hebbeln, D., Arz, H.W., Stoner, J., 2004. Antarctic timing of surface water changes off Chile and Patagonian Ice Sheet response. Science 304, 1959–1962.
Lamy, F., Arz, H.W., Kilian, R., Lange, C.B., Lembke-Jene, L., Wengler, M., Kaiser, J., Baeza-Urrea, O., Hall, I.R., Harada, N., Tiedemann, R., 2015. Glacial reduction and millennial scale variations in Drake Passage throughflow. Proc. Natl. Acad. Sci. U. S. A. 112, 13496–13501.
Lifton, N., Sato, T., Dunai, T., 2014. Scaling in situ cosmogenic nuclide production rates using analytical approximations to atmospheric cosmic-ray fluxes. Earth Planet Sci. Lett. 386, 149–160.
Luckman, B.H., Villalba, R., 2001. Assessing the synchroneity of glacier fluctuations in the western cordillera of the Americas during the Last Millennium. In: Markgraf, V. (Ed.), Interhemispheric Climate Linkages. Academic Press, pp. 119–140.
Mackintosh, A.N., Anderson, B.M., Pierrehumbert, R.T., 2017. Reconstructing climate from glaciers. Annu. Rev. Earth Planet Sci. 45, 649–680.
Marden, C.J., Clapperton, C.M., 1995. Fluctuations of the south patagonian icefield during the last glaciation and the Holocene. J. Quat. Sci. 10, 197–210.
Marshall, G.J., Orr, A., van Lipzig, N.P.M., King, J.C., 2006. The impact of a changing Southern Hemisphere annular mode on Antarctic Peninsula summer temperatures. J. Clim. 19, 5388–5404.
Marshall, G.J., Speer, K., 2012. Closure of the meridional overturning circulation through Southern Ocean upwelling. Nat. Geosci. 5, 171–180. https://doi.org/10.1038/NGEO1391.
Martinson, D.G., Stammerjohn, S.E., Ianuzzi, R.A., Smith, R.C., Vernet, M., 2008. Western Antarctic Peninsula physical oceanography and spatio-temporal variability. Deep-Sea Res. II 55, 1964_1987.
Masiokas, M.H., Rivera, A., Espizua, L.E., Villalba, R., Delgado, S., Aravena, J.C., 2009. Glacier fluctuations in extratropical South America during the past 1000 years. Palaeogeogr. Palaeoclimatol. Palaeoecol. 281, 242–268.
Masiokas, M., Casteller, A., Villalba, R., Trombotto, D., Ripalta, A., Hernandez, J., Lázaro, M., 2000. Latitudinal differences in glacier fluctuations across Patagonia: a dendrogeomorphological approach to characterize climate variability in the southern Andes during the past 1000 years (PATAGON-1000). In: Abstracts from the International Conference on Dendrochronology for the Third Millennium. Mendoza, Argentina, p. 176.
Masiokas, M., Villalba, R., Delgado, S., Trombotto, D., Luckman, B., Ripalta, A., Hernandez, J., 2001. Dendrogeomorphological reconstruction of glacier variations in northern Patagonia during the past 1000 years. In: Kaennel Dobbertin, M., Bräker, O.U. (Eds.), Abstracts from the International Conference on Tree Rings and People. Davos, Switzerland, p. 177.
Meier, W.J.-H., Grießinger, J., Hochreuther, P., Braun, M.H., 2018. An updated multitemporal glacier inventory for the Patagonian Andes with changes between the Little Ice Age and 2016. Front. Earth Sci. 6 (62), 1–21.
Menounos, B., Maurer, L., Clague, J.J., Osborn, G., 2020. Late Holocene fluctuations of Stoppani glacier, southernmost Patagonia. Quat. Res. 95, 56–64.
Mercer, J.H., 1965. Glacier variations in southern Patagonia. Geogr. Rev. 55, 390–413.
Mercer, J.H., 1968. Variations of some Patagonian glaciers since the Late glacial I. Am. J. Sci. 266, 91–109.
Mercer, J.H., 1970. Variations of some patagonian glaciers since the late-glacial: II. Am. J. Sci. 269, 1–25.
Mercer, J.H., 1982. Holocene glacier variation in southern South America. Striae 18, 35–40.
Moreno, P.I., François, J.P., Villa-Martínez, R.P., Moy, C.M., 2009. Millennial-scale variability in Southern Hemisphere westerly wind activity over the last 5000 years in SW Patagonia. Quat. Sci. Rev. 28, 25–38.
Moreno, P.I., Francois, J.P., Villa-Martínez, R., Moy, C.M., 2010. Covariability of the southern westerlies and atmospheric CO2 during the Holocene. Geology 39, 727–730.
Moreno, P.I., Vilanova, I., Villa-Martinez, R., Garreaud, R.D., Rojas, M., De Pol-Holz, 2014. Southern Annular Mode-like changes in southwestern Patagonia at centennial timescales over the last three millenia. Nat. Commun. 5, 4375. https://doi.org/10.1038/ncomms5375.
Moreno, P.I., Vilanova, I., Villa-Martínez, R., Dunbar, R.B., Mucciarone, D.A., Kaplan, M.R., Garreaud, R.D., Rojas, M., Moy, C.M., De Pol-Holz, R., Lambert, F., 2018. Onset and evolution of southern annular mode-like changes at centennial timescale. Sci. Rep. 8, 3458.
Moy, C.M., Dunbar, R.B., Moreno, P.I., Francois, J.P., Villa-Martínez, R., Mucciarone, D.M., Guilderson, T.P., Garreaud, R.D., 2008. Isotopic evidence for hydrologic change related to the westerlies in SW Patagonia, Chile, during the last millennium. Quat. Sci. Rev. 27, 1335–1349.
Nimick, D.A., McGrath, D., Mahan, S.A., Friesen, B.A., Leidich, J., 2016. Latest pleistocene and Holocene glacial events in the Colonia valley, northern Patagonia icefield, southern Chile. J. Quat. Sci. 31, 551–564.
Nishiizumi, K., Imamura, M., Caffee, M.W., Southon, J.R., Finkel, R.C., McAninch, J., 2007. Absolute calibration of ^{10}Be AMS standards. Nucl. Instrum. Methods Phys. Res. B 258, 403–413.
Oerlemans, J., 2005. Extracting a climate signal from 169 glacier records. Science 29, 675–677.
Piotrowski, J.A., Larsen, Nicolaj K., Jung, Frank W., 2004. Reflections on soft subglacial beds as a mosaic of deforming and stable spots. Quat. Sci. Rev. 23, 993–1000.
Pike, Jennifer, George, E.A. Swann, Leng, Melanie J., Snelling, Andrea M., 2013. Glacial discharge along the West Antarctic Peninsula during the Holocene. Nat. Geosci. 6, 199–202.
Porter, S.C., 2000. Onset of neoglaciation in the southern hemisphere. J. Quat. Sci. 15, 395–408.
Previdi, M., Polvani, L.M., 2014. Climate system response to stratospheric ozone depletion and recovery. Quart. J. Roy. Meteor. Soc. 140, 2401–2419.
Pritchard, H.D., Ligtenberg, S.R.M., Fricker, H.A., Vaughan, D.G., van den Broeke, M.R., Padman, L., 2012. Antarctic ice-sheet loss driven by basal melting of ice shelves. Nature 484, 502–505.
Putnam, A.E., Schaefer, J.M., Denton, G.H., Barrell, D.J.A., Finkel, R.C., Andersen, B.G., Schwartz, R., Chinn, T.J.H., Doughty, A.L., 2012. Regional climate control of glaciers in New Zealand and Europe during the pre-industrial Holocene. Nat. Geosci. 5, 627–630.
Reynhout, S.A., Sagredo, E.A., Kaplan, M.R., Aravena, J.C., Martini, M.A., Moreno, P.I., Rojas, M., Schwartz, R., Schaefer, J.M., 2019. Quat. Sci. Rev. 220, 178–187.
Röthlisberger, F., 1986. 10, 000 Jahre Gletschergeschichte der Erde. Verlag Sauerländer, Aarau.
Rignot, E., Rivera, A., Casassa, G., 2003. Contribution of the Patagonia icefields of south America to sea level rise. Science 302, 434–436.
Rignot, E., Mouginot, J., Scheuchl, B., van den Broeke, M., van Wessem, M.J., Morlighem, M., 2019. Four decades of Antarctic ice sheet mass balance from 1979–2017. Proc. Natl. Acad. Sci. Unit. States Am. 116, 1095–1103.
Rivera, A., Casassa, G., 2004. Ice elevation, areal, and frontal changes of glaciers from National Park Torres del Paine, Southern Patagonia Icefield Arctic. Antarct. Alp. Res. 36, 379–389.
Sagredo, E.A., Rupper, S., Lowell, T.V., 2014. Sensitivities of the equilibrium line altitude to temperature and precipitation changes along the Andes. Quat. Res. 81 (2), 355–366.
Sagredo, E.A., Lowell, T.V., Kelly, M.A., Rupper, S., Aravena, J.C., Ward, D.J., Malone, A.G., 2016. Equilibrium line altitudes along the Andes during the Last millennium: paleoclimatic implications. Holocene 27, 1019–1033.
Schaefer, J.M., Denton, G.H., Kaplan, M.R., Putnam, A.P., Finkel, R.C., Barrell, D.J.A.,

Andersen, B.G., Schwartz, R., Mackintosh, A., Chinn, T., Schlücter, C., 2009. High frequency Holocene glacier fluctuations in New Zealand differ from the northern signature. Science 324, 622–625.
Schneider, C., Glaser, M., Kilian, R., Santana, A., Butorovic, N.G., 2003. Weather observations across the southern Andes at 53_S. Phys. Geogr. 24, 97–119.
Shevenell, A.E., Kennett, J.P., 2002. Antarctic Holocene climate change: a benthic foraminiferal stable isotope record from Palmer Deep. Palaeoceanography 17, 1019.
Stone, J.O., 2000. Air pressure and cosmogenic isotope production. J. Geophys. Res. 105, 23753–23759.
Strelin, J., Casassa, G., Rosqvist, G., Holmlund, P., 2008. Holocene glaciations in the ema glacier valley, Monte Sarmiento Massif, Tierra del Fuego. Palaeogeogr. Palaeoclimatol. Palaeoecol. 260, 299–314.
Strelin, J.A., Kaplan, M.R., Vandergoes, M.J., Denton, G.H., Schaefer, J.M., 2014. Holocene glacier history of the Lago Argentino Basin, southern patagonian icefield. Quat. Sci. Rev. 101, 124–145.
Stuiver, M., 1978. Atmospheric Carbon dioxide and Carbon reservoir changes. Science 199 (4326), 253–258.
Stuiver, M., Pearson, G.W., 1993. High precision bidecadal calibration of the radiocarbon time-scale, A.D. 1950-500 B.C. and 2500-6000 B.C. Radiocarbon 35, 1–24.
Thompson, D.W.J., Solomon, S., 2002. Interpretation of recent Southern Hemisphere climate change. Science 296, 895–899.
Thompson, D.W.J., Solomon, S., Kushner, P.J., England, M.H., Grise, K.M., Karoly, D.J., 2011. Signatures of the Antarctic ozone hole in Southern Hemisphere surface climate change. Nat. Geosci. 4, 741.
Toggweiler, J.R., Russell, J.L., Carson, S.R., 2006. Midlatitude westerlies, atmospheric CO_2, and climate change during the ice ages. Paleoceanography 21, PA2005. https://doi.org/10.1029/2005PA001154.
Turton, J.V., Kirchgaessner, A., Ross, A.N., King, J.C., 2018. The spatial distribution and temporal variability of föhn winds over the Larsen C ice shelf, Antarctica. Q. J. R. Meteorol. Soc. 144, 1169–1178. https://doi.org/10.1002/qj.3284.
Villalba, R., 1990. Climatic fluctuations in northern Patagonia in the last 1000 years as inferred from tree ring records. Quat. Res. 34, 346–360.
Villalba, R., 1994. Tree-ring and glacial evidence for the Medieval warm epoch and the Little ice age in southern South America. Clim. Change 26, 183–197.
Villalba, R., Masiokas, M., Kitzberger, T., Boninsegna, J.A., 2005. Biogeographical consequences of recent climate changes in the southern Andes of Argentina. In: Global Change and Mountain Regions: an Overview of Current Knowledge. Series: Advances in Global Change Research, vol. 23, pp. 157–166.
Walker, M.J.C., Berkelhammer, M., Bjö Rck, S., Cwynar, L.C., Fisher, D.A., Long, A.J., Lowe, J.J., Newnham, R.M., Rasmussen, S.O., Weiss, H., 2012. Formal subdivision of the Holocene Series/epoch: a discussion paper by a working group of INTIMATE (integration of ice-core, marine and terrestrial records) and the Subcommission on quaternary stratigraphy (international Commission on stratigraphy). J. Quat. Sci. 27, 649–659.
Wiles, G.C., Barclay, D.J., Calkin, P.E., Lowell, T.V., 2008. Century to millennial-scale temperature variations for the last two thousand years indicated from glacial geologic records of Southern Alaska. Global Planet. Change 60, 115–125.
Yuan, X., Kaplan, M.R., Cane, M.A., 2018. The interconnected global climate system—a review of tropical–polar teleconnections. J. Clim. 31, 5765–5792.
Zumbühl, H.J., Nussbaumer, S.U., 2018. Little Ice Age glacier history of the central and western Alps from pictorial documents. Cuadernos de Investigación Geográfica 44, 115–136.